JACS
JOURNAL OF THE AMERICAN CHEMICAL SOCIETY

ARTICLE

pubs.acs.org/JACS

Transfer, Amplification, and Inversion of Helical Chirality Mediated by Concerted Interactions of C_3-Supramolecular Dendrimers

Mihai Peterca,[†,‡] Mohammad R. Imam,[†] Cheol-Hee Ahn,[†] Venkatachalapathy S. K. Balagurusamy,[†] Daniela A. Wilson,[†] Brad M. Rosen,[†] and Virgil Percec*[,†]

[†]Roy & Diana Vagelos Laboratories, Department of Chemistry, University of Pennsylvania, Philadelphia, Pennsylvania 19104-6323, United States

[‡]Department of Physics and Astronomy, University of Pennsylvania, Philadelphia, Pennsylvania 19104-6396, United States

Supporting Information

ABSTRACT: The synthesis, structural, and retrostructural analysis of two libraries containing 16 first and second generation C_3-symmetric self-assembling dendrimers based on dendrons connected at their apex via trisesters and trisamides of 1,3,5-benzenetricarboxylic acid is reported. A combination of X-ray diffraction and CD/UV analysis methods demonstrated that their C_3-symmetry modulates different degrees of packing on the periphery of supramolecular structures that are responsible for the formation of chiral helical supramolecular columns and spheres self-organizable in a diversity of three-dimensional (3D) columnar, tetragonal, and cubic lattices. Two of these periodic arrays, a 3D columnar hexagonal superlattice and a 3D columnar simple orthorhombic chiral lattice with $P222_1$ symmetry, are unprecedented for supramolecular dendrimers. A thermal-reversible inversion of chirality was discovered in helical supramolecular columns. This inversion is induced, on heating, by the change in symmetry from a 3D columnar simple orthorhombic chiral lattice to a 3D columnar hexagonal array and, on cooling, by the change in symmetry from a 2D hexagonal to a 2D centered rectangular lattice, both exhibiting intracolumnar order. A first-order transition from coupled columns with long helical pitch, to weakly or uncorrelated columns with short helical pitch that generates a molecular rotator, was also discovered. The torsion angles of the molecular rotator are proportional to the change in temperature, and this effect is amplified in the case of the C_3-symmetric trisamide supramolecular dendrimers forming H-bonds along their column. The structural changes reported here can be used to design complex functions based on helical supramolecular dendrimers with different degree of packing on their periphery.

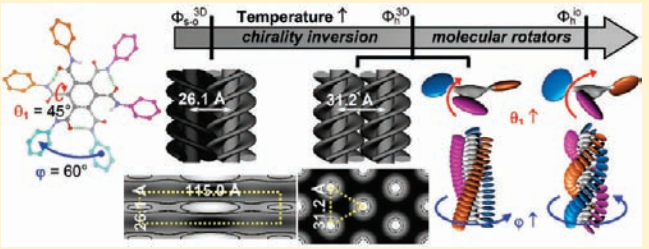

INTRODUCTION

Supramolecular helical structures generated from self-assembling dendrons,[1] dendrimers,[2] and other macromolecules[3] are of interest for a diversity of areas, including optics,[4] molecular recognition,[5] nanotubes,[6] folding,[3a,7] nanomachines,[8] porous protein mimic,[1] and organic electronics.[9] Interest in these supramolecular assemblies is fueled by the high level of control that can be achieved in the design of the building blocks,[3] which can facilitate a precise incorporation of functional groups in various parts of the helix.[1,10] Nevertheless, there are many examples of helical structures that have the potential to act as scaffolds for nanoscale applications,[11] but which upon subsequent functionalization might lose their original spatial organization.[12] Therefore, full exploration of the potential of these systems requires a complete understanding of how helicity emerges through transfer of structural information[13] from the molecular to the supramolecular,[14] and from the supramolecular to the periodic or quasi-periodic array levels.

Herein, we exploit the intrinsic propensity of self-assembling dendrimers with 3-fold symmetry[15] to form helical supramolecular structures[2e] and investigate the mechanism of transfer of structural information from the molecular to supramolecular level, and from the supramolecular to the three-dimensional periodic or quasi-periodic level. Using a combination of powder and oriented fiber X-ray diffraction (XRD), electron density Fourier reconstructions,[16] numerical and molecular model based simulations of the XRD,[2e] differential scanning calorimetry (DSC), circular dichroism, and UV spectroscopy (CD/UV−vis) techniques applied in solid state, we identified an unexpected diversity of three-dimensional (3D) columnar, tetragonal, and cubic arrays self-organized from C_3-symmetric dendrimers. This combination of techniques facilitated the elucidation of the mechanism of transfer, amplification, and inversion of helical chirality that occurs upon heating at the transition from a new orthorhombic chiral phase with $P222_1$ symmetry to a 3D hexagonal columnar phase Φ_h^{3D}. The inversion of chirality[17] is thermal-reversible, occurring upon cooling at the transition from columnar hexagonal to columnar centered rectangular phase. This inversion is determined by the symmetry of the 3D periodic organization,

Received: November 30, 2010
Published: January 31, 2011

Scheme 1. Structure and Synthesis of 1,3,5-Bz-Trisester and 1,3,5-Bz-Trisamide Dendrimers[a]

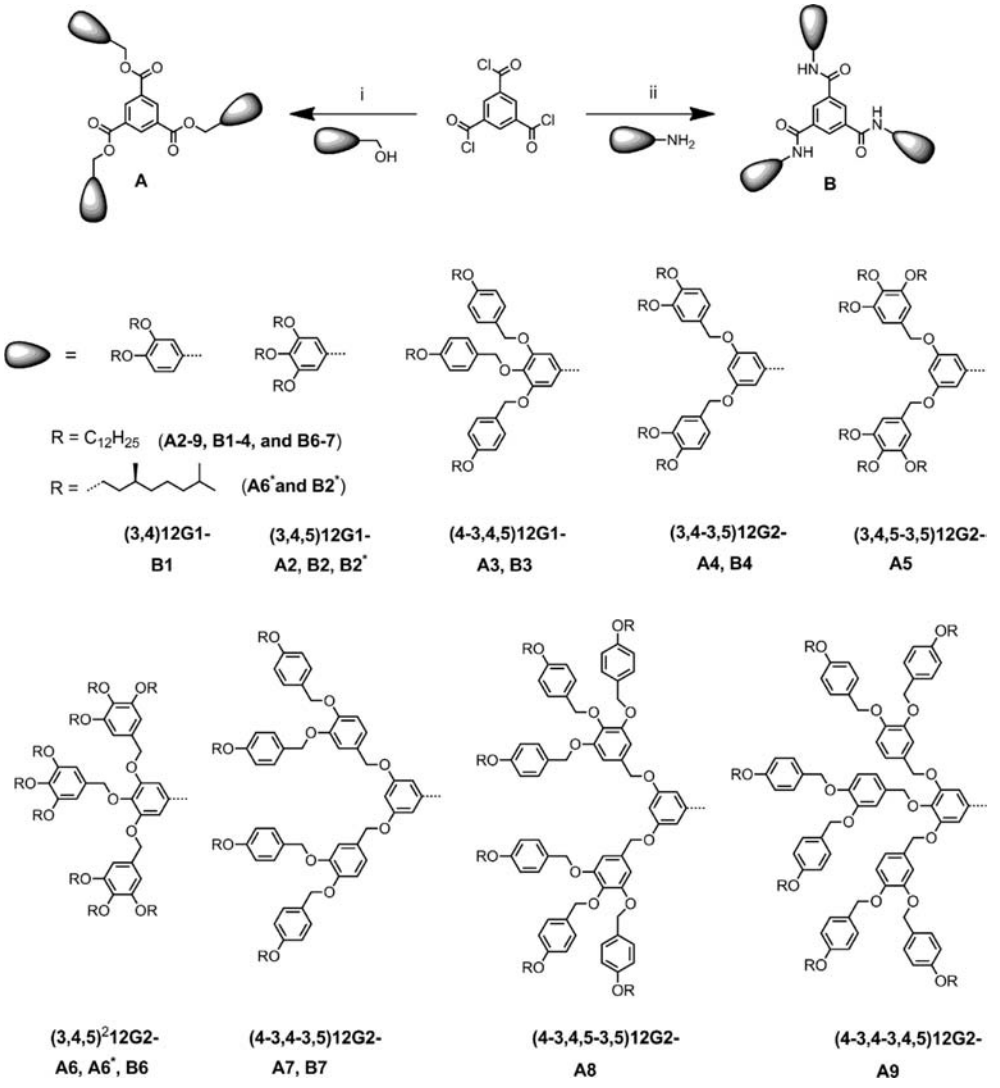

[a] Reagents and conditions: (i) DMAP, CH_2Cl_2, room temperature, 8−12 h, 50−70%; (ii) DTBMP, CH_2Cl_2, room temperature, 6 h, 65−75%.

illustrating the importance of chirality transfer at the lattice level. In addition, such 3D correlations between helical columns limit the helical growth and template unusual slow advancing helices characterized by a long pitch. Furthermore, a molecular rotator[18] was demonstrated to occur via temperature change at the first-order transition from coupled helical columns with long helical pitch to uncoupled helical columns with short helical pitch. The motion of the molecular rotator is reversible and can be tuned via the incorporation of amide groups at the dendrimer apex to amplify the conformational changes via the formation of directional intracolumnar H-bonds. The transfer, amplification, and inversion of chirality reported here provide a fundamentally new approach to the amplification of chirality.[19] Other helical supramolecular systems have been found to exhibit inversion of helical chirality in response to changes in temperature,[17a,17b] solvent,[17b] or the concentration of the chiral dopant molecules used in the coassembly.[19e] Nevertheless, to our knowledge, this is the first example of chirality inversion templated by the symmetry of the self-organized 3D packing. While previous examples of chiral inversion could be rationalized on the basis of thermodynamics and kinetics, the detailed structural information provided in this solid-state inversion of chirality provides the first case wherein a molecular mechanism of the inversion processes is demonstrated.

The trisester and trisamide dendrimers form chiral spherical supramolecular structures by pathways similar to those of other C_3-symmetric dendrimers, such as dendronized cyclotriveratrylene and triphenylene.[15c,15d] The unexpected formation of a diversity of columnar and helical structures, with or without intercolumnar correlations, is attributed to the less-densely packed periphery of the supramolecular dendrimers and to the increased conformational freedom of the dendritic branches of the trisester and trisamide dendrimers by contrast with dendrimers with 3-fold symmetry characterized by a more densely packed periphery generated via dendritic hexasubstitution of cyclotriveratrylene[2e,15c] and triphenylene.[15d]

Scheme 2. Synthesis of Chiral Amine (3,4,5)dm8*G1−NH_2 (4)[a]

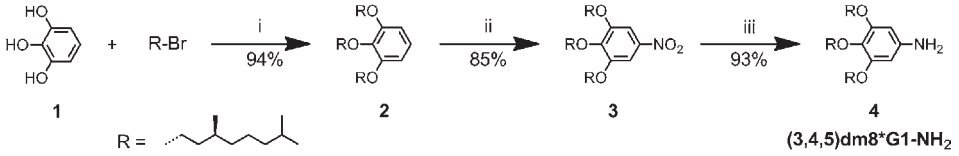

[a] Reagents and conditions: (i) K_2CO_3, DMF, 60 °C, 4 h; (ii) $SiO_2 \cdot HNO_3$, CH_2CI_2, room temperature, 15 min; (iii) $NH_2NH_2 \cdot H_2O$, graphite, EtOH, reflux, 24 h.

Scheme 3. Synthesis of Second Generation Dendritic Amines[a]

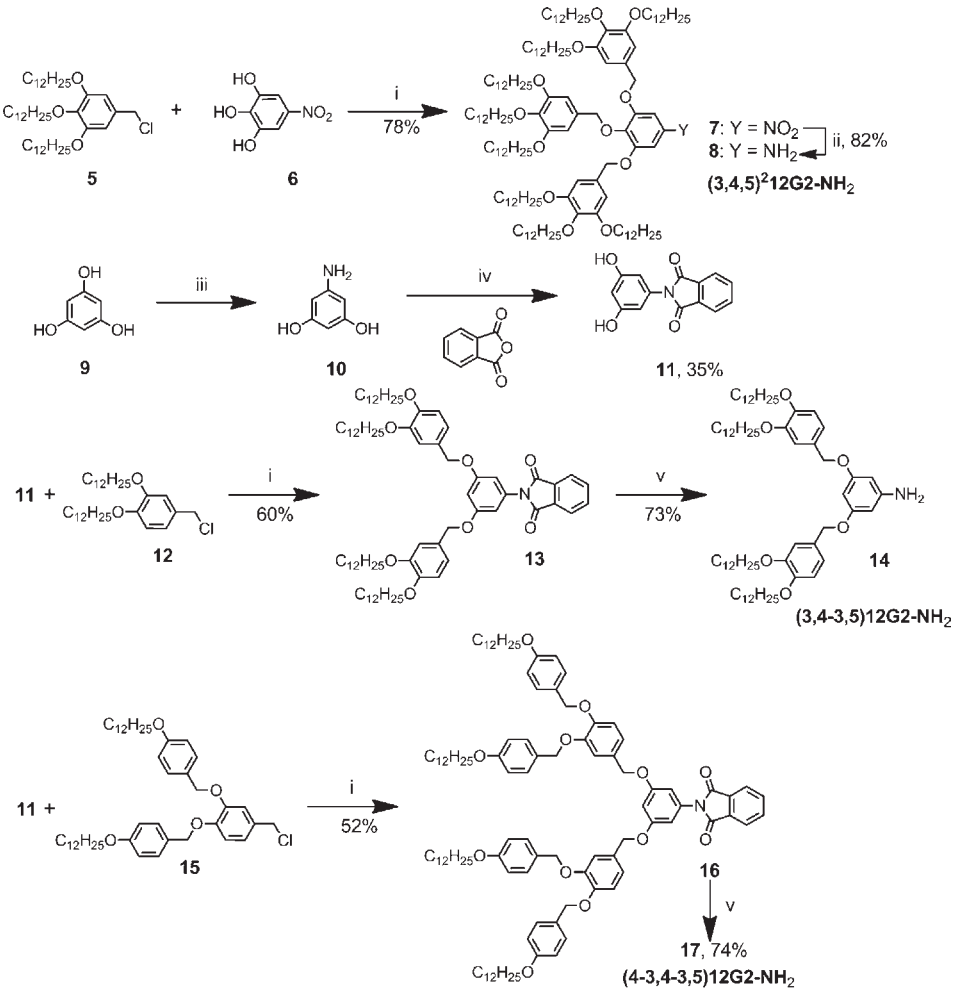

[a] Reagents and conditions: (i) K_2CO_3, DMF, 70 °C, 12 h; (ii) $NH_2NH_2 \cdot H_2O$, graphite, EtOH−THF, reflux, 24 h; (iii) NH_4OH, 50 °C, 12 h; (iv) KOAc, AcOH, reflux, 1.5 h; (v) $NH_2NH_2 \cdot H_2O$, graphite, EtOH−THF, reflux, 2 h.

RESULTS AND DISCUSSION

Synthesis. Two libraries of self-assembling dendrimers containing nine trisester (**A2**−**9**, **A6***) and seven trisamide groups at their apex (**B1**−**4**, **6**, **7**, and **B2***) were synthesized through the symmetric esterification or amidation of nine different achiral and chiral dendrons to a central 1,3,5-benzenetricarboxylic acid core (Scheme 1).

The nine self-assembling dendrons forming the periphery of dendrimers were designed with primary structures that will probe the effect of branching pattern on the type of 2D liquid crystalline and 3D phases they will form.[20] For the synthesis of all dendrimers, a convergent iterative process based on accelerated synthetic methods elaborated in our laboratory was employed.[21] The first step of the synthesis of self-assembling trisester dendrimers requires dendrons possessing a benzyl alcohol at their apex. These benzyl alcohols were esterified with 1,3,5-benzenetricarbonyl trichloride in CH_2Cl_2 using catalytic 4-dimethylamino pyridine (DMAP) in moderate yields. Similarly, the first step of the synthesis of self-assembling trisamide dendrimers required dendrons possessing an aryl amine at their apex. These aryl amines were amidated with 1,3,5-benzenetricarbonxyl

dx.doi.org/10.1021/ja110753s |J. Am. Chem. Soc. 2011, 133, 2311–2328

Table 1. Thermal Analysis of the Supramolecular Dendrimers Self-Assembled from Trisesters and Trisamides

compound	phase transition (°C) and corresponding enthalpy changes (kcal mol^{-1})[a] heating	cooling
1,3,5-Bz-[tris(3,4,5)12G1]-trisester (**A2**)	Φ_x 49.0 (33.64) i Φ_x 1.1 (2.59) Φ_x 39.8 (−9.10) Φ_x 49.0 (29.76) i	i 31.0 (−12.04) Φ_x −2.6 (−2.46) Φ_x
1,3,5-Bz-[tris(4−3,4,5)12G1]-trisester (**A3**)	Φ_h^{3D} −16.3 (9.77) Φ_h^{3D} 46.6 (0.89) Φ_h^{io} 192.5 (20.18) i Φ_h^{3D} −6.7 (8.45) Φ_h^{3D} 71.6 (1.09) Φ_h^{io} 191.9 (18.42) i	i 184.6 (−18.65) Φ_h^{io} 64.2 (−1.01) Φ_h^{io} −11.0 (−6.75) Φ_h^{3D}
1,3,5-Bz-[tris(4−3,4−3,5)12G2]-trisester (**A7**)	Φ_h^{io} −13.3 (16.53) Φ_h^{io} 147.6 (1.93) Φ_h 161.6 (9.44) i Φ_h^{io} −11.2 (16.30) Φ_h^{io} 146.4 (1.93) Φ_h 161.3 (9.22) i	i 159.2 (−9.14) Φ_h 145.2 (−1.45) Φ_h^{io} −25.5 (−38.55) Φ_h^{io}
1,3,5-Bz-[tris(4−3,4,5−3,5)12G2]-trisester (**A8**)	Φ_h^{io} 46.2 (0.96) Φ_h^{io} 116.4 (1.48) Tet 149.9 (0.39) i Φ_h^{io} 117.2 (2.62) Tet 140.1 (0.65) i	i 134.2 (−0.53) Tet 104.0 (−2.43) Φ_h^{io}
1,3,5-Bz-[tris(4−3,4−3,4,5)12G2]-trisester (**A9**)	Φ_h^{io} −16.4 (14.89) Φ_h^{io} 99.1 (1.79) Cub 209.5 (0.52) Tet 253[b] dec Φ_h^{io} −14.8 (11.28) Φ_h^{io} 110.4 (2.10) Cub 165.2 (0.87) Cub 207.6 (0.15) Tet 250[b] dec	dec 195.9 (−0.01) Cub 144.6 (−1.75) Φ_h^{io}
1,3,5-Bz-[tris(3,4−3,5)12G2]-trisester (**A4**)	$\Phi_h^{3D\text{-}1}$ 37.4 (2.23) $\Phi_h^{3D\text{-}2}$ 67.5 (26.75) $\Phi_h^{3D\text{-}3}$ 93.0 (13.11)[c] i $\Phi_h^{3D\text{-}1}$ 2.2 (13.44) $\Phi_h^{3D\text{-}2}$ 20.8 (1.32) $\Phi_h^{3D\text{-}3}$ 93.2 (15.25)[c] i	i 86.1 (−13.93) $\Phi_h^{3D\text{-}3}$ 18.5 (−1.25) $\Phi_h^{3D\text{-}2}$ −3.7 (−11.36) $\Phi_h^{3D\text{-}1}$
1,3,5-Bz-[tris(3,4,5−3,5)12G2]-trisester (**A5**)	Φ_h 42.8 (5.59) $\Phi_h^{3D\text{-}SL}$ 70.1 (29.17) i Φ_h 38.6 (−11.18) $\Phi_h^{3D\text{-}SL}$ 70.6 (35.35) i	i 56.3 (−0.99) $\Phi_{r\text{-}c}$ 42.3 (−2.98) Φ_h 27.0 (−2.17) Φ_h
1,3,5-Bz-[tris(3,4,5)^{2}12G2]-trisester (**A6**)	x −14.1 (5.85) g[d] 42.1 (2.67) Cub 121.4 (1.32) i x −16.6 (15.60) g[d] 19.0 (4.48) Cub 121.3 (1.38) i	i 47.9 (−0.48) Cub 3.0 g[d]
1,3,5-Bz-[tris(3,4,5)^{2}dm8*G2]-trisester (**A6***)	T_g 7.6 Cub 74.7 (1.25) i T_g 11.4 Cub 74.7 (1.15) i	i 109.2 (−0.94) Cub −20.1 (−16.47) T_g
1,3,5-Bz-[tris(3,4)12G1]-trisamide (**B1**)	Φ_x 80.2 (24.91) Φ_h^{io} 250.7 (2.55) i Φ_x −1.2 (4.65) Φ_x 78.6 (0.93) Φ_h^{io} 250.5 (2.42) i	i 247.7 (−2.34) Φ_h^{io} 51.3 (−0.64) Φ_x −6.2 (−2.44) Φ_x
1,3,5-Bz-[tris(3,4,5)12G1]-trisamide (**B2**)	$\Phi_{r\text{-}s}^{o}$ −1.5 (9.29) $\Phi_{r\text{-}s}^{o}$ 57.4 (0.65) Φ_h^{3D} 94[b] Φ_h^{io} 178.8 (6.29) i $\Phi_{r\text{-}s}^{o}$ −3.9 (10.63) $\Phi_{r\text{-}s}^{o}$ 61.0 (0.53) Φ_h^{3D} 103.6 (0.53) Φ_h^{io} 179.0 (6.50) i	i 175.0 (−6.13) Φ_h^{io} 82[d] Φ_h^{3D} −9.6 (−5.00) $\Phi_{r\text{-}s}^{o}$
1,3,5-Bz-[tris(3,4,5)dm8*G1]-trisamide (**B2***)	$\Phi_{s\text{-}o}^{o}$ 40[b] Φ_h^{3D} 88.3 (0.63) Φ_h^{io} 108.3 (2.39) i $\Phi_{s\text{-}o}^{o}$ 40[b] Φ_h^{3D} 86.0 (0.46) Φ_h^{io} 108.3 (1.95) i	i 102.6 (−1.92) Φ_h^{io} 78.7 (−0.53) $\Phi_{r\text{-}c}^{io}$ 40[b] $\Phi_{s\text{-}o}^{o}$
1,3,5-Bz-[tris(4−3,4,5)12G1]-amide (**B3**)	$\Phi_{r\text{-}s}^{o}$ 174.6 (1.17) Φ_h 212.7 (3.83) i $\Phi_{r\text{-}s}^{o}$ 152.0 (0.79) Φ_h 204.1 (1.25) i	i 208.6 (−1.20) Φ_h 146.5 (−0.48) $\Phi_{r\text{-}s}^{o}$
1,3,5-Bz-[tris(3,4−3,5)12G2]-trisamide (**B4**)	Φ_h^{o} 44.7 (12.83) T_g 81.9 Φ_h 116.4 (2.10) i Φ_h^{o} 6.0 (10.76) T_g 78.8 Φ_h 116.4 (2.05) i	i 111.2 (−2.66) Φ_h 1.0 (−8.48) Φ_h^{o}
1,3,5-Bz-[tris(4−3,4−3,5)12G2]-trisamide (**B7**)	Φ_h^{o} −9.9 (7.76) Φ_h^{o} 58.2 (0.55) Φ_h^{io} 189.7 (3.00) i Φ_h^{o} −6.1 (7.55) Φ_h^{io} 159.1 (2.81) i	i 151.8 (−2.38) Φ_h^{io} −13.0 (−8.78) Φ_h^{o}
1,3,5-Bz-[tris(3,4,5)^{2}12G2]-trisamide (**B6**)	g[d] −8.8 (23.47) g[d] 95.4 (2.59) Cub 178.1 (1.10) i g[d] −11.0 (23.24) Cub 177[b] i	i 169[b] Cub −15.0 (−27.32) g[d]

[a] Data from the first heating and cooling scans are on the first line, and data from the second heating are on the second line; Φ_h, hexagonal columnar phase; Φ_h^{io}, columnar hexagonal phase with intracolumnar order; Φ_h^{3D}, columnar hexagonal phase with three-dimensional order; $\Phi_h^{3D\text{-}SL}$, three-dimensional columnar hexagonal superlattice; Φ_x, unidentified columnar lattice; $\Phi_{r\text{-}c}$, centered rectangular columnar phase; $\Phi_{r\text{-}c}^{io}$, centered rectangular columnar phase with intracolumnar order; $\Phi_{r\text{-}s}^{o}$, simple rectangular ordered columnar phase; $\Phi_{s\text{-}o}^{o}$, simple orthorhombic ordered columnar phase; Tet, $P4_2/mnm$ tetragonal LC phase; Cub, $Pm\bar{3}n$ cubic phase; T_g, glass transition; i, isotropic; dec, decomposition. [b] This transition is observed only by TOPM and XRD. [c] Sum of enthalpies from overlapped peaks. [d] Glassy $Pm\bar{3}n$ cubic phase as observed by XRD.

trichloride in CH_2Cl_2 using 2,6-di-*tert*-butyl-4-methylpyridine (DTBMP) as base.

The synthesis of the three dendritic amines employed in the construction of compounds **B1**, **B2**, and **B3** was reported previously.[22] The chiral amine for the triamide **B2*** was synthesized following the identical literature procedure (Scheme 2).[22a] Specifically, pyrogallol was trisalkylated with (*R*)-2,7-dimethyloctyl (dm8*) bromide in excellent yield (94%). Nitration of the alkylated pyrogallol proceeded rapidly using SiO_2 pretreated with nitric acid (85% yield). Finally, (3,4,5)dm8*G1−NH_2 was achieved in very good yield (93%) through reduction of nitro group with hydrazine hydrate.

The three new dendritic amines required for the synthesis of trisamides **B4**, **B6**, and **B7** were prepared through similar methods (Scheme 3). 3,4,5-Tris(3,4,5-tris-dodecyloxy-benzyloxy)-phenyl amine, (3,4,5)^{2}12G2−NH_2 (**8**), was obtained in two steps from the dendritic chloride, **5**, and the known[22a,22c] compound 1,2,3-trihydroxy-5-nitrobenzene (**6**). The aryl nitro group from intermediate **7** was reduced by $NH_2NH_2 \cdot H_2O$ using graphite catalyst to give the dendritic amine **8** in 82% yield. The N-protected dihydroxy aniline **11** was obtained from phloroglucinol **9** via successive monoamination with ammonium hydroxide and imidization with phthalic anhydride

Table 2. Phases, Lattice Parameters, and Measured *d*-Spacing of the Trisester Dendrimers

dendrimer	T (°C)	phase[a]	a, b, c (Å)[b]	d_{100}, d_{110}, d_{200}, d_{210}, d_{300}, d_{220}, d_{310}, d_{400}, d_{320} (Å)[c] d_{410}, d_{401}, d_{321}, d_{113}, d_{303}, d_{223}, d_{403}, d_{0010} (Å)[d] d_{002}, d_{112}, d_{202}, d_{003}, d_{004}, d_{205}, d_{007}, d_{008}, d_{009}, d_{0017} (Å)[e] d_{10}, d_{11}, d_{20}, d_{21}, d_{30}, d_{22} (Å)[f] d_{002}, d_{410}, d_{330}, d_{411}, d_{421} (Å)[g] d_{110}, d_{200}, d_{210}, d_{211}, d_{220}, d_{310}, d_{321}, d_{400} (Å)[h] d_{200}, d_{220}, d_{400}, d_{301}, d_{102} (Å)[i] d_{20}, d_{04}, d_{24}, d_{33}, d_{40}[k]
1,3,5-Bz-[tris(4−3,4,5)12G1]-trisester	25	Φ_h^{3D}	42.4, −, 33.5	36.7, −, 18.4, 13.9, 12.2, 10.6, 10.2, 9.2, 8.4[c]
				8.0, 8.9, 8.2, 9.9, 8.2, 7.7, 7.1, 3.4[d]
	170	Φ_h^{io}	44.9	38.9, −, 19.4, 14.7, 12.9, 11.2[f]
1,3,5-Bz-[tris(3,4,5)12G1]-trisester	45	Φ_x		29.1[j]
	20	Φ_x		32.4[j]
1,3,5-Bz-[tris(4−3,4−3,5)12G2]-trisester	25	Φ_h^{io}	57.6	50.0, 28.8, 24.9[f]
	120	Φ_h^{io}	55.6	48.3, 27.8, 24.0[f]
	155	Φ_h	53.1	46.1, 26.5, 23.0[f]
1,3,5-Bz-[tris(4−3,4,5−3,5)12G2]-trisester	80	Φ_h^{io}	51.2	44.3, 25.5, 22.1[f]
	140	$P4_2/mnm$	167.2, −, 96.4	48.2, 40.6, 39.4, 37.4[g]
1,3,5-Bz-[tris(4−3,4−3,4,5)12G2]-trisester	25	Φ_h^{io}	54.8	47.6, 27.3, 23.7[f]
	210	$Pm\bar{3}n$	102.3	−, 51.2, 45.8, 41.7, 36.2, −, 27.2, 25.5[h]
	240	$P4_2/mnm$	179.9, −, 96.5	48.3, 43.6, −, 39.8, 37.1[g]
1,3,5-Bz-[tris(3,4−3,5)12G2]-trisester	−25	$\Phi_h^{3D\text{-}1}$	44.5, −, 23.0	38.5, 22.3, 19.3[c]
				11.5, −, 9.9, 7.7, −, −, 3.3[e]
	12	$\Phi_h^{3D\text{-}2}$	44.6, −, 55.6	38.6, 22.3, 19.3[c]
				−, −, −, −, 13.9, 9.6, −, 7.0, 6.2, 3.3[e]
	80	$\Phi_h^{3D\text{-}3}$	44.8, −, 23.8	38.8, 22.4, 19.4[c]
				−, 10.5, −, −, −, −, 3.4[e]
1,3,5-Bz-[tris(3,4,5−3,5)12G2]-trisester	10	Φ_h	43.9	38.1, 21.9, 19.0[f]
	57	$\Phi_h^{3D\text{-}SL}$	87.7, −, 71.9	37.9, 21.9, 18.9, 23.9, 32.5[i]
	53[l]	$\Phi_{r\text{-}c}$	74.3, 103.9	37.2, 26.0, 21.3, 20.1, 18.6[k]
1,3,5-Bz-[tris(3,4,5)^{2}12G2]- trisester	25	X		36.2[j]
	105	$Pm\bar{3}n$	72.4	51.2, 36.2, 32.4, 29.6, 25.6, 22.9, 19.3, 18.1[h]
1,3,5-Bz-[tris(3,4,5)^{2}dm8*G2]-trisester	20	$Pm\bar{3}n$	63.3	−, 31.6, 28.3, 25.8[h]
	65	$Pm\bar{3}n$	62.8	−, 31.4, 28.1, 25.6[h]

[a] Phase notation: Φ_h, columnar hexagonal phase; Φ_h^{io}, columnar hexagonal phase with intracolumnar order; Φ_h^{o}, columnar hexagonal ordered phase; Φ_h^{3D}, $\Phi_h^{3D\text{-}1}$, $\Phi_h^{3D\text{-}2}$, and $\Phi_h^{3D\text{-}3}$, three-dimensional columnar hexagonal phases; $\Phi_{r\text{-}c}$, centered rectangular columnar phase; Φ_x, unidentified columnar phase; x, unidentified phase; $P4_2/mnm$, tetragonal phase; $Pm\bar{3}n$, cubic phase; $\Phi_h^{3D\text{-}SL}$, three-dimensional columnar hexagonal superlattice. [b] Lattice parameters calculated using $d_{hkl} = 1/(4(h^2 + k^2 + hk)/(3a^2) + l^2/c^2)^{1/2}$ for hexagonal phases, $d_{hk} = 1/(h^2/a^2 + k^2/b^2)^{1/2}$ for rectangular phases, $d_{hkl} = a/(h^2 + k^2 + l^2)^{1/2}$ for cubic phases, and $d_{hkl} = 1/((h^2 + k^2)/a^2 + l^2/c^2)^{1/2}$ for tetragonal phases. [c,d,e,f,i] d-spacing for columnar hexagonal phases. [g] d-spacing for tetragonal phases. [h] d-spacing for cubic phases. [j] d-spacing for unidentified phase. [k] d-spacing for centered rectangular phases. [l] $\Phi_{r\text{-}c}$ phase observed only upon cooling from the isotropic phase.

(35% two-step yield). The etherification of **11** with dendritic chloride **12** in the presence of anhydrous K_2CO_3 in DMF provided compound **13**, which was then reduced to the desired amine, 3,5-bis-[3,4-bis-(dodecyloxy)-benzyloxy] aniline, (3,4−3,5)12G2-NH_2 (**14**), in 73% yield. Similarly, 3,5-bis-[3,4-bis-(4-dodecyloxy-benzyloxy)-benzyloxy] aniline, (4−3,4−3,5)12G2-NH_2 (**17**), was synthesized from **11** and chloride **15** in good yield.

Structural and Retrostructural Analysis. Tables 1, 2, and 3 summarize the combined analysis of the self-assembling C_3-symmetric dendrimers in the solid state via a combination of differential scanning calorimetry (DSC), thermal polarized optical microscopy, small (SAXS), and wide (WAXS)-angle powder and oriented fiber X-ray diffraction experiments. Assignment of various new and unusual columnar lattices reported in Tables 1, 2, and 3 was facilitated by X-ray diffraction data methods, simulation techniques established previously for the columnar hexagonal and centered rectangular phases with intracolumnar order (Φ_h^{io} and $\Phi_{r\text{-}c}^{io}$, respectively),[2d,7,16] and through the development of new Fourier series reconstructions of the electron density distributions for the columnar hexagonal phase with 3D order (Φ_h^{3D}), columnar hexagonal superlattice with 3D order ($\Phi_h^{3D\text{-}SL}$), and the simple columnar orthorhombic phase with 3D order ($\Phi_{s\text{-}o}^{3D}$). In combination with thin film CD/UV spectroscopy and molecular modeling, the mechanism of self-assembly and self-organization process into a variety of helical supramolecular columnar and spherical assemblies was elucidated.

On the basis of the phases presented in Tables 1, 2, and 3, the self-assembly process of C_3 dendrimers can be directly correlated

dx.doi.org/10.1021/ja110753s |J. Am. Chem. Soc. 2011, 133, 2311–2328

Table 3. Phases, Lattice Parameters, and Measured *d*-Spacing of the Trisamide Dendrimers

dendrimer	T (°C)	phase[a]	a, b, c (Å)[b]	$d_{10}, d_{11}, d_{20}, d_{21}$ (Å)[c] $d_{100}, d_{101}, d_{111}, d_{102}$ (Å)[d] $d_{01}, d_{10}, d_{11}, d_{21}$ (Å)[e] $d_{200}, d_{210}, d_{211}, d_{220}, d_{310}, d_{321}, d_{400}$ (Å)[f] $d_{010}, d_{110}, d_{210}, d_{401}, d_{202}, d_{311}, d_{402}$ (Å)[g] $d_{006}, d_{008}, d_{0012}$ (Å)[h] d_{20}, d_{11} (Å)[i]
1,3,5-Bz-[tris(3,4)12G1]-trisamide	95	Φ_h^{io}	32.4	28.2, 16.2[c]
	35	Φ_x		32.5[i]
1,3,5-Bz-[tris(3,4,5)12G1]-trisamide	20	$\Phi_{r\text{-}s}^{o}$	66.1, 30.1	30.1, −, 27.4, 22.3[e]
	60	Φ_h^{3D}	36.4, −, 54.2	31.5, 27.2, 17.3, 20.6[d]
	110	Φ_h^{io}	34.4	29.8, 17.2[c]
1,3,5-Bz-[tris(4−3,4,5)12G1]-trisamide	140	$\Phi_{r\text{-}s}^{o}$	29.9, 39.3	39.3, 29.9[e]
	170	Φ_h	29.9	33.9[c]
1,3,5-Bz-[tris(4−3,4−3,5)12G2]-trisamide	20	Φ_h^{o}	51.0	44.2, 25.4, 22.2[c]
	140	Φ_h^{io}	50.5	43.7, 25.2, 21.8[c]
1,3,5-Bz-[tris(3,4−3,5)12G2]-trisamide	25	Φ_h^{io}	43.8	38.0[c]
	90	Φ_h	42.9	37.1[c]
1,3,5-Bz-[tris(3,4,5)^{2}12G2]-trisamide	25	$Pm\bar{3}n$	69.8	34.3, 31.0, 28.4[f]
	120	$Pm\bar{3}n$	73.6	36.9, 33.0, 30.1, 25.9, 19.6, 18.5[f]
1,3,5-Bz-[tris(3,4,5)dm8*G1]-trisamide	25	$\Phi_{s\text{-}o}^{3D}$	115.0, 26.1, 50.9	26.1, 25.5, 23.8, 25.0, 23.3, 19.9, 19.1[g] 8.5, 6.4, 4.2[h]
	75	Φ_h^{3D}	31.2, −, 77.3	27.0, 25.5, −, 22.1[d]
	95	Φ_h^{io}	29.0	25.1, 14.5[c]
	65[j]	$\Phi_{r\text{-}c}^{io}$	52.2, 26.9	52.2, 26.9[i]

[a] Phase notation: Φ_h, columnar hexagonal phase; Φ_h^{io}, columnar hexagonal phase with intracolumnar order; Φ_h^{3D}, three-dimensional columnar hexagonal phases; $Pm\bar{3}n$, cubic phase; Φ_x, unidentified phase; $\Phi_{r\text{-}c}^{io}$, centered rectangular columnar phase with intracolumnar order; $\Phi_{r\text{-}s}^{o}$, simple rectangular ordered columnar phase; and $\Phi_{s\text{-}o}^{3D}$, simple orthorhombic 3D ordered columnar phase with $P222_1$ symmetry. [b] Lattice parameters calculated using $d_{hkl} = 1/(4(h^2 + k^2 + hk)/(3a^2) + l^2/c^2)^{1/2}$ for hexagonal phases, $d_{hk} = 1/(h^2/a^2 + k^2/b^2)^{1/2}$ for rectangular phases, $d_{hkl} = a/(h^2 + k^2 + l^2)^{1/2}$ for cubic phases, and $d_{hkl} = 1/(h^2/a^2 + k^2/b^2 + l^2/c^2)^{1/2}$ for the simple orthorhombic columnar phase with $P222_1$ symmetry. [c,d] *d*-spacing for hexagonal phases. [e] *d*-spacing for simple rectangular phases. [f] *d*-spacing for cubic phases. [g,h] *d*-spacing for the simple orthorhombic phase. [i] *d*-spacing for centered rectangular phase. [j] Phase observed only upon cooling from the isotropic phase.

with the primary structure of their dendritic branches. Columnar hexagonal, rectangular, and orthorhombic phases are predominantly formed by self-organization of dendrimers based on the first generation dendrons (Tables 1, 2, and 3). C_3 dendrimers based on second generation dendrons also self-assemble into columnar phases at low temperatures, with the exception of the two trisester and one trisamide dendrimers based on the $(3,4,5)^2$-G2 dendrons, which exhibit the $Pm\bar{3}n$ cubic phase.[21c,23,24] Remarkably, two dendrimers based on second generation dendrons, 1,3,5-Bz-[tris(4−3,4,5−3,5)12G2]-trisester and 1,3,5-Bz-[tris(4−3,4−3,4,5)12G2]-trisester, exhibit at high temperatures the tetragonal phase with $P4_2/mnm$ symmetry, which is rarely observed in self-assembling dendrons,[25a] dendrimers,[15c,d] and other macromolecules.[25b,25c]

Molecular Design Principles for Supramolecular Columns with Long Helical Pitch. The analysis of the wide-angle X-ray diffraction (WAXS) patterns collected from the oriented fibers of 1,3,5-Bz-[tris(4−3,4,5)12G1]-trisester, presented in Figure 1, demonstrated the formation of a Φ_h^{3D} phase at low temperatures (25 °C), and a Φ_h^{io} phase at high temperatures (170 °C). Interestingly, the diffraction features of the fiber WAXS patterns can be indexed as $L = 0$, 3, 7, and 10, even upon heating through the first-order transition from Φ_h^{3D} (Figure 1a) to Φ_h^{io} (Figure 1b). Alternatively, the layer lines observed in the WAXS fiber pattern of the Φ_h^{io} phase (Figure 1b) can be indexed as $L = 0$, 2, 5, and 7 (Figure 1c). These two indexing schemes correspond to two possible helices, triple-30_1 and triple-21_1,[2e,7] respectively (Figure 1c).

The atomistic simulations[2e,7] of the triple-30_1 and triple-21_1 supramolecular columns (Figure 1c) demonstrate that the position of the maxima of the layer lines observed in the experimental XRD fiber pattern (Figure 1b) is well fit by both simulations. Therefore, the definitive assessment of the helical packing of the supramolecular columns self-assembled from 1,3,5-Bz-[tris(4−3,4,5)12G1]-trisester required the simulation of the oriented fiber patterns calculated from the two alternative molecular models (Supporting Information, Figure SF1). From the simulation, the triple-30_1 (Figure 2) helical packing provided the best fit of the experimental fiber WAXS data of the Φ_h^{io} phase (Figure 1b). Furthermore, the average correlation length of the intracolumnar order, ξ, calculated from the width of the π-stacking features indicated in Figure 1a and b is $\xi \approx 60$ column strata for both the Φ_h^{3D} and the Φ_h^{io} phases (Figure 1d). These results demonstrate that upon the first-order transition from the Φ_h^{3D} phase, formed by strongly coupled helical columns, to the Φ_h^{io} phase, formed by weakly or uncoupled helical columns, the internal helical packing of the supramolecular columns is unchanged.

The unusual slow advancing helical arrangement (Figure 2a) can be attributed to the specific topology of the dendritic unit,

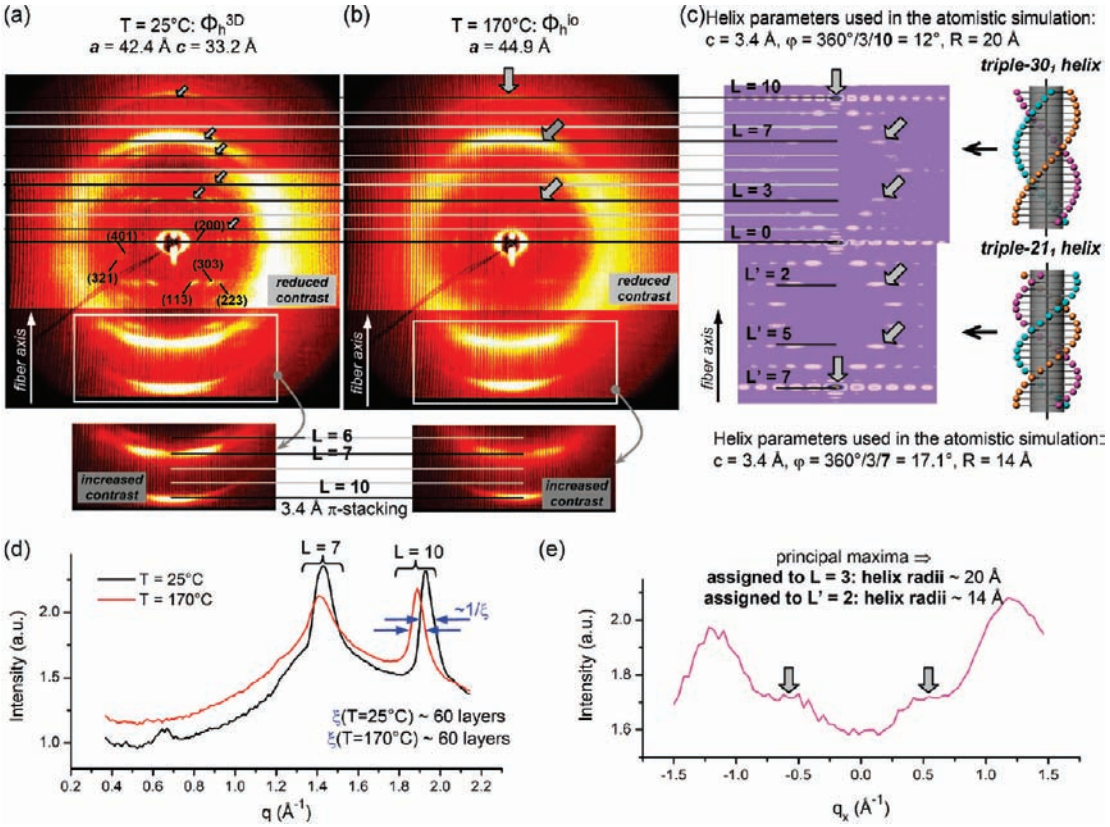

Figure 1. Wide-angle X-ray scattering patterns collected from the oriented fiber of 1,3,5-Bz-[tris(4−3,4,5)12G1]-trisester in the Φ_h^{3D} (a) and Φ_h^{io} (b) phases. Simulations of WAXS fiber pattern from (b) based on the two simplified atomistic models (c). Meridional plots of the corresponding WAXS fiber patterns (d) and plot integrating the region of the first layer line with nonzero intensity of the WAXS fiber pattern shown in b (e). In parts a,b, the layer lines absent or with very weak intensity profiles are colored in gray.

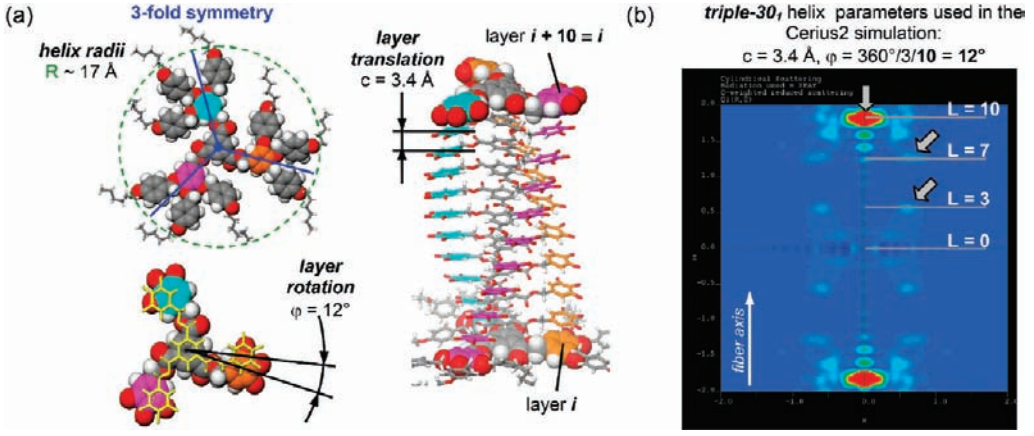

Figure 2. Detail of the supramolecular helical columns of 1,3,5-Bz-[tris(4−3,4,5)12G1]-trisester in the Φ_h^{io} phase (a) established from atomistic and molecular model-based simulation (b) of the WAXS oriented fiber patterns.

which facilitates a smaller angle of rotation of the adjacent layers, $\varphi = 12°$. As a comparison, the peripheries of these trisubstituted C_3-symmetric dendrimers are less packed than the periphery of the hexasubstituted dendronized cyclotriveratrylene and triphenylene reported previously.[15c,15d] Therefore, the helical parameter φ of the C_3-symmetric dendrimers with "filled" periphery[15c,15d] varied between 30 and 60°, whereas in the case of 1,3,5-Bz-[tris(4−3,4,5)12G1]-trisester this parameter is at least 3 times smaller ($\varphi = 12°$, Figures 1 and 2). Similarly, slow advancing helical packing in combination with strong column-to-column correlations[26] can explain the remarkable 3D columnar hexagonal superlattice, $\Phi_h^{3D\text{-}SL}$, and the columnar hexagonal 3D phases observed, respectively, in the second generation 1,3,5-Bz-[tris(3,4,5−3,5)12G2]-trisester and 1,3,5-Bz-[tris(3,4−3,5)12G2]-trisester dendrimers (Figures 3, 4, and Supporting Information Figure SF6).

dx.doi.org/10.1021/ja110753s |J. Am. Chem. Soc. 2011, 133, 2311–2328

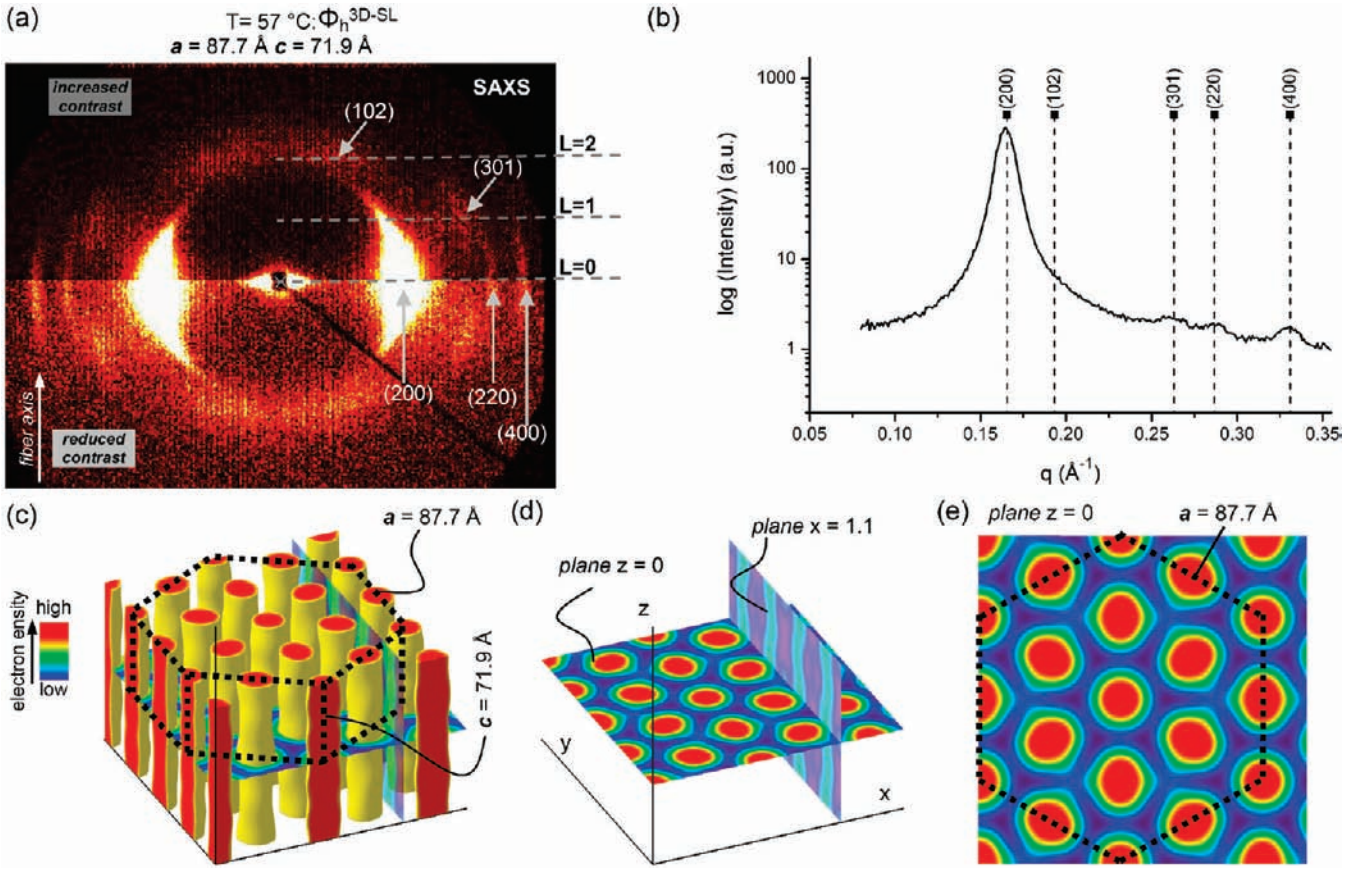

Figure 3. SAXS pattern collected from the oriented sample of 1,3,5-Bz-[tris(3,4,5−3,5)12G2]-trisester in the $\Phi_h^{3D\text{-}SL}$ phase (a), corresponding intensity versus scattering vector plot (b), reconstructed relative electron density distribution (c), and two representative planar cross sections of the volumetric distribution from (c) are detailed in (d) and (e), as indicated.

The formation of the 3D columnar hexagonal superlattice can be attributed to the close packing of undulated columns,[26] as suggested by the reconstructed relative electron density distribution and maps presented in Figure 3c−e. The oriented fiber XRD pattern collected at small angles from 1,3,5-Bz-[tris(3,4,5−3,5)-12G2]-trisester (Figure 3a) exhibits very weak and broad (*hkl*) diffraction peaks in the case of $l \neq 0$, demonstrating that the long-range column-to-column correlations, which span in average about 10−14 × *c* unit cells, are relatively weak. On the other hand, the oriented fiber WAXS pattern exhibits strong off-meridional features on the $L = 6$ layer, demonstrating stronger short-range column-to-column correlations (Supporting Information Figure SF7). Therefore, the hexagonal columnar superlattice is generated via coupling of undulated columns that are highly ordered within the length scale of the unit cell. Interestingly, after "removing"[26] one alkyl chain from the dendritic building block, the 1,3,5-Bz-[tris(3,4−3,5)12G2]-trisester exhibits a 3D columnar hexagonal phase with a shorter *c* axis of 55.6 Å (Figure 4), in comparison with *c* = 71.9 Å observed for the 1,3,5-Bz-[tris(3,4,5−3,5)12G2]-trisester. At the same time, the average thickness of the column stratum was reduced from 4.4 to 3.4 Å. These results demonstrate that the rotational angle of the adjacent column stratum was slightly reduced from 120°/16 = 7.5° to 120°/17 = 7.1°. Furthermore, the torsion angle θ_1 characterizing the propeller like conformation of the dendron, which will be discussed in the next section, was reduced in direct correlation to the degree of the intramolecular steric constraints generated by a less-packed alkyl periphery.

The 1,3,5-Bz-[tris(3,4−3,5)12G2]-trisester exhibits an unusual sequence of 3D columnar hexagonal phases. Figure 4 illustrates the $\Phi_h^{3D\text{-}2}-\Phi_h^{3D\text{-}3}$ transition, which is accompanied by a reduction of the *c*-axis of the 3D columnar hexagonal phases from 55.6 to 23.8 Å. This reduction can be associated with an increase of the rotational angle of the adjacent column strata associated with increasing temperature. Such an increase is typically correlated with a larger dendron solid angle[16a,27] and possibly with the increase of its θ_1 torsion angle upon the increase of temperature. Additional examples of C_3-symmetric dendrimers that exhibit an increase of the rotational angle of the adjacent column strata and of the θ_1 torsion angle upon the increase of temperature will be discussed in the next section.

Thermal-Reversible Inversion of Chirality in Supramolecular Columns Mediated by Lattice Symmetry Changes. The achiral 1,3,5-Bz-[tris(3,4,5)12G1]-trisamide dendrimer self-organizes at low temperatures into a 3D columnar hexagonal phase (Figure 5) and at high temperatures into a columnar hexagonal phase with intracolumnar order (Φ_h^{io}). Both WAXS fiber patterns exhibit similar diffuse and broad features in the wide-angle region (Figure 5a and Supporting Information Figure SF3a), which demonstrate that in both phases the supramolecular columns are jacketed by an aliphatic region with a liquid-like structure. Remarkably, when the same dendritic branching pattern is decorated with chiral chains on the periphery, 1,3,5-Bz-[tris(3,4,5)dm8*G1]-trisamide, the self-organization process templates a new simple orthorhombic 3D phase, $\Phi_{s\text{-}o}^{3D}$

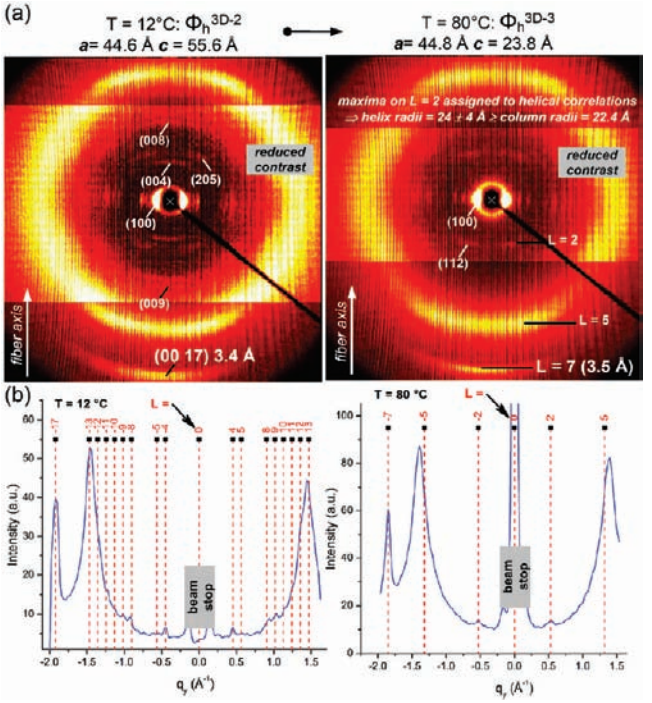

Figure 4. Wide-angle X-ray scattering patterns collected in the second heating of the oriented fiber of 1,3,5-Bz-[tris(3,4−3,5)12G2]-trisester at the indicated temperatures (a) and corresponding q_y plots (b).

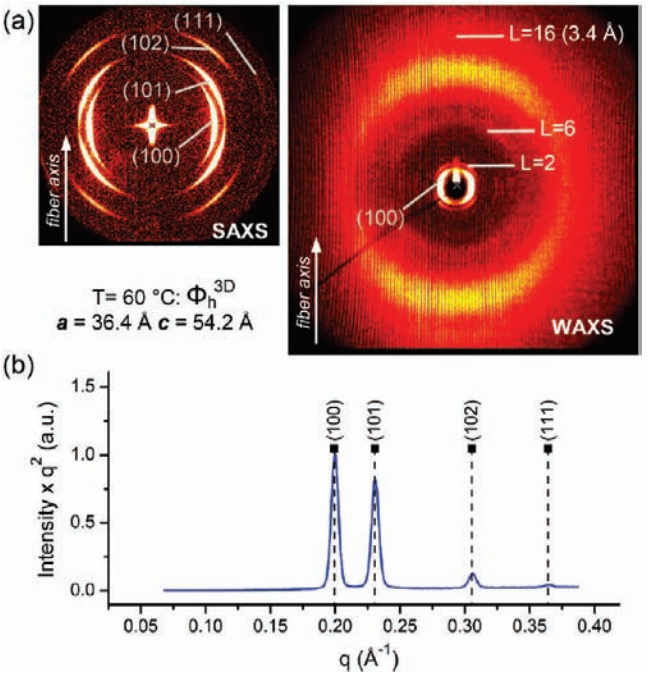

Figure 5. Small and wide-angle X-ray scattering patterns collected in the Φ_h^{3D} phase of 1,3,5-Bz-[tris(3,4,5)12G1]-trisamide at the indicated temperature (a) and the corresponding plot (b).

(Figure 6), at low temperatures, while preserving the Φ_h^{3D} and Φ_h^{io} phases observed at higher temperature (Figure 7).

Figure 6 presents the wide- and small-angle XRD data, as well as the approximate relative electron density distribution within the $z = 0$ plane of the new $\Phi_{s\text{-}o}^{3D}$ phase. The indexing of the small angle XRD fiber pattern (Figure 6a,c) is consistent with $P222_1$ symmetry. The proposed relative electron density distribution (Figure 6d) can only be approximated because the $\Phi_{s\text{-}o}^{3D}$ phase is noncentrosymmetric[16] and only the amplitudes of the ($hk0$) diffraction peaks were included in the Fourier series reconstruction. In contrast with the high temperature Φ_h^{3D} and Φ_h^{io} phases (Figure 7), the wide-angle region of the fiber pattern collected in the low temperature simple orthorhombic ordered phase exhibits sharp diffraction features (Figure 6b and Supporting Information Figures SF4, SF5). These features demonstrate the presence of long-range intra- and intercolumnar correlations and also that the aliphatic region jacketing the columns has significantly lower conformational freedom in the $\Phi_{s\text{-}o}^{3D}$ phase. Therefore, the addition of chiral centers to the alkyl chains induced strong coupling of the helical supramolecular columns and templates the formation of the new simple orthorhombic lattice with $P222_1$ chiral symmetry.

Figure 8a details the DSC traces collected with 10°/min from the 1,3,5-Bz-[tris(3,4,5)dm8*G1]-trisamide. Interestingly, the $\Phi_{s\text{-}o}^{3D}-\Phi_h^{3D}$ transition upon heating and the $\Phi_h^{io}-\Phi_{r\text{-}c}^{io}$ transition upon cooling indicated in Figure 8a were observed in the XRD and CD experiments (Figures 6, 7, and 9) but not in the DSC traces collected with either slow (1°/min) or fast (10°/min) rates. CD and XRD experiments were used to study upon heating and cooling the chiral 1,3,5-Bz-[tris(3,4,5)dm8*G1]-trisamide dendrimer in the solid state (Figures 8b,c and 9). No linear dichroism was observed in these perfectly reproducible experiments. In the low temperature $\Phi_{s\text{-}o}^{3D}$ phase, the CD spectrum exhibits a Cotton effect with the maximum at 222 nm and a negative one with the maximum at 203 nm. At the same time, the UV−vis spectrum displays a maximum absorption positioned at 212 nm, at the midpoint between these two Cotton effects with opposite sign (Figure 8b,c). These results indicate a positive exciton coupling[28] and demonstrate that the supramolecular columns self-organized in the $\Phi_{s\text{-}o}^{3D}$ phase are helical.

Remarkably, upon subsequent heating, above ~35 °C in the Φ_h^{3D} phase, the exciton coupling changes its sign from positive to negative (Figure 9a). The negative exciton coupling is preserved upon subsequent heating, above the temperature of the $\Phi_h^{3D}-\Phi_h^{io}$ first-order phase transition, but the intensities of the two Cotton effects observed at 198 and 224 nm, respectively, are reduced by a factor of ~6. In combination with the WAXS fiber data (Figure 7), these results suggest that the supramolecular columns of the Φ_h^{3D} and Φ_h^{io} phase are helical and that the Φ_h^{3D} phase was templated by undulations of the soft liquid-like aliphatic periphery. Precedent for the helical arrangement of the aliphatic region on the periphery of supramolecular columns is available.[29] These undulations are generated by the helical packing of the aromatic core region of the supramolecular columns, which translate into periodic variations of the aliphatic periphery. Furthermore, in the low temperature simple orthorhombic phase, the degree of column-to-column correlation increased to the extent of favoring a structure with $P222_1$ chiral symmetry, exhibiting the opposite positive exciton coupling (Figures 9 and 10).

Upon cooling through the $\Phi_h^{io}-\Phi_{r\text{-}c}^{io}$ transition temperature, the CD spectra exhibit another inversion of chirality, from a positive to a negative exciton coupling. The intensity of the two Cotton effects (Figure 9b) is weak in both phases, in direct correlation with the diffuse and broad features observed in the wide-angle region of their oriented fiber XRD patterns (Figure 7). Upon further cooling, the exciton coupling stays positive in the

dx.doi.org/10.1021/ja110753s |J. Am. Chem. Soc. 2011, 133, 2311–2328

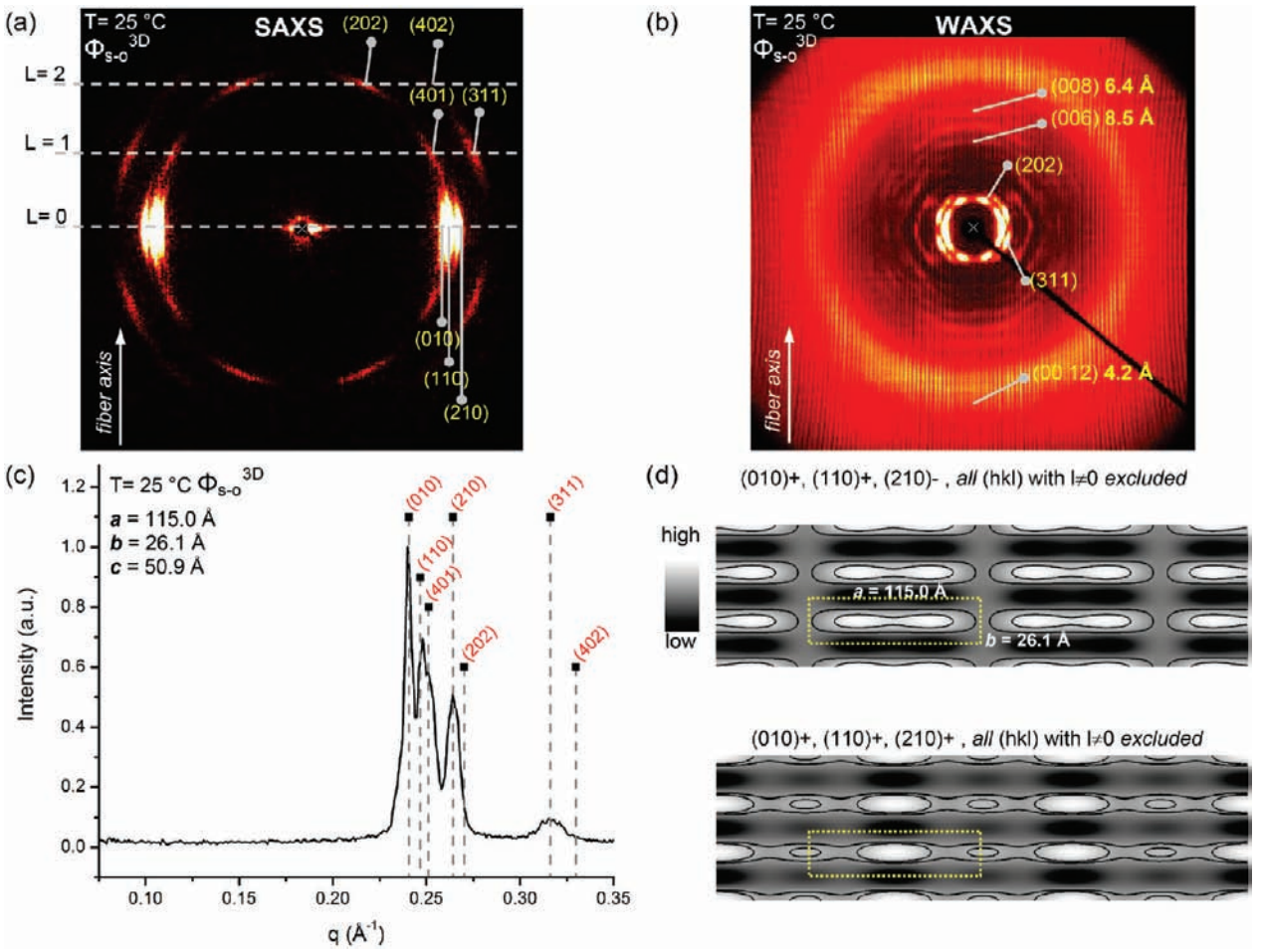

Figure 6. SAXS (a) and WAXS (b) patterns collected from the oriented sample of 1,3,5-Bz-[tris(3,4,5)dm8*G1]-trisamide in the $\Phi_{s\text{-}o}^{3D}$ phase with $P222_1$ symmetry observed at T < 35 °C. Intensity versus scattering vector plot of the fiber pattern from (a), diffraction peaks indexing, and lattice parameters (c). Two alternative electron density maps of the plane z = 0 of the $\Phi_{s\text{-}o}^{3D}$ phase (d).

$\Phi_{s\text{-}o}^{3D}$ phase, as expected, but the two Cotton effects exhibit an increase of their intensity by a factor of ~5. Through the combination of the electron density maps, phase assignment, and the sign of the exciton coupling (Figure 10), a direct correlation between the chirality of the supramolecular columns and the symmetry of their three-dimensional packing is found. Consistently, in the "triangular" phases, Φ_h^{3D} and Φ_h^{io}, which are formed by weakly or uncoupled helical columns, their chirality is negative, whereas in the rectangular phases, $\Phi_{s\text{-}o}^{3D}$ and $\Phi_{r\text{-}c}^{io}$, their chirality is positive. These results imply that the stronger column-to-column correlations established in the $\Phi_{s\text{-}o}^{3D}$ phase play an important role in favoring one dominant handedness.

Nearly all the self-organizable C_3-symmetric dendrimers reported here are achiral and would therefore provide no dichroic signal in their helical supramolecular structure. However, 1,3,5-Bz-[tris(3,4,5)dm8*G1]-trisamide (**B2***), for example, is chiral, and, therefore, its self-assembly in solution was probed by CD/UV−vis experiments performed in solvophobic solvents. In agreement with previous studies performed in heptane at 10^{-4}−10^{-5} M,[15a] **B2*** did not exhibit any Cotton effects when the CD/UV−vis spectra were collected in the same range of concentration in the temperature range 8−25 °C from a variety of other solvophobic solvents, including hexane, methylcyclohexane, dodecane, buthanol, nor from the good solvents tetrahydrofuran and chloroform. While previously documented by Meijer,[15a] the absence of any CD response in solution is somewhat surprising considering the significant intensity of the Cotton effects observed in solid state and the typically observed direct correspondence between helical self-assembly of chiral supramolecular dendrimers in solution and in thin film.[1,15c,15d]

The analysis of the WAXS fiber data shown (Figures 7 and SF5), demonstrated that upon the Φ_h^{3D}−Φ_h^{io} first-order phase transition the π-stacking distance is shifted from ~3.6 to ~3.9 Å. This result, in combination with CD spectroscopy on film (Figures 8 and 9) and molecular modeling, provided the limit of the torsion angles proposed in Figures 11 and 12. Upon the transition from the Φ_h^{3D} phase, formed by coupled columns, to the Φ_h^{io} phase, formed by weakly or uncoupled columns, the decoupling of columns release the steric constraints, which limited the helical parameter to values of φ<15°, and driven by the tendency to form directional hydrogen bonds, this parameter increases in the Φ_h^{io} phase to φ = 60°. At the same time, the torsion angle θ_1 is increased from values smaller than 30° to about 45° (Figures 11 and 12). Therefore, upon the Φ_h^{3D}−Φ_h^{io} first-order phase transition, the supramolecular dendrimers undergo rotation mediated by the formation of directional H-bonds

dx.doi.org/10.1021/ja110753s |*J. Am. Chem. Soc.* 2011, 133, 2311–2328

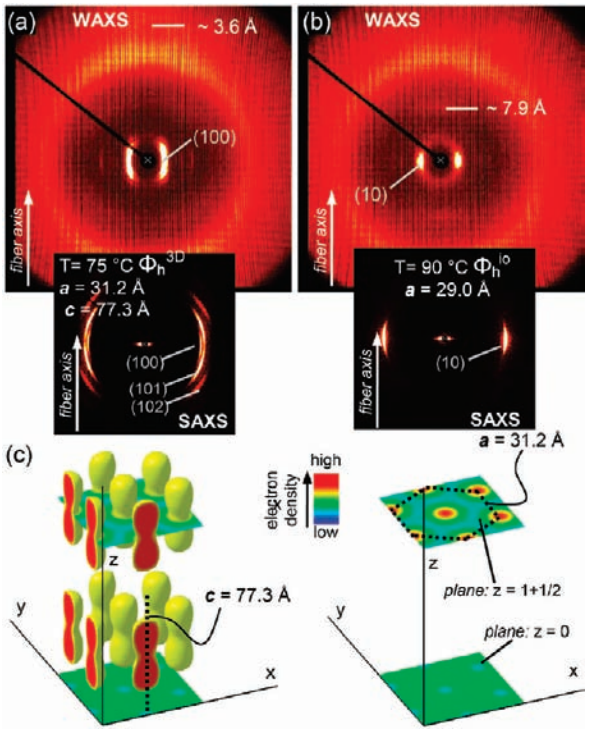

Figure 7. WAXS and SAXS patterns collected from the oriented sample of 1,3,5-Bz-[tris(3,4,5)dm8*G1]-trisamide in the Φ_h^{3D} (a) and Φ_h^{io} (b) phases. Reconstructed relative electron density distributions of the Φ_h^{3D} phase (c).

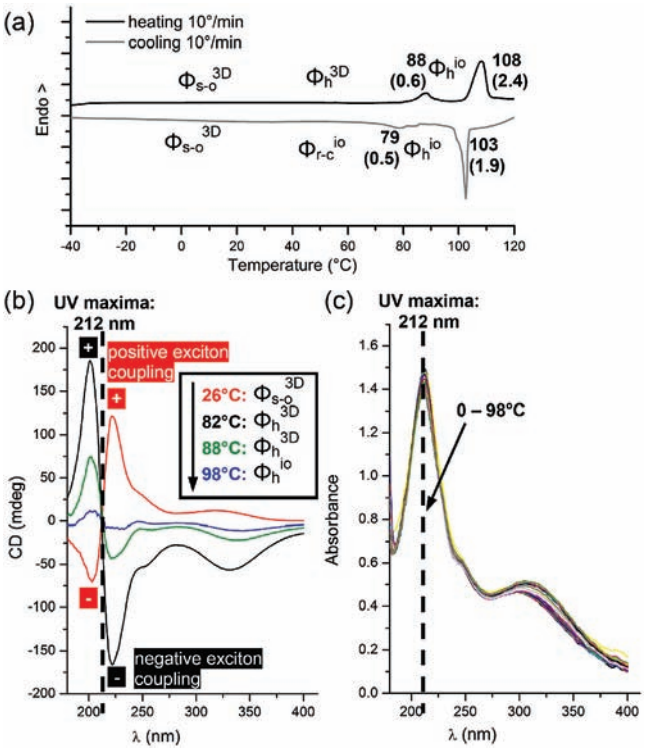

Figure 8. Differential scanning calorimetry traces collected with 10°/min from 1,3,5-Bz-[tris(3,4,5)dm8*G1]-trisamide (a). CD (b) and UV (c) spectra of 1,3,5-Bz-[tris(3,4,5)dm8*G1]-trisamide in spin-coated film cast from hexane (concentration = 2.0%, w/v) collected on heating. In (a) phases, phase transition temperatures and associated enthalpy changes (in brackets in kcal/mol) are indicated. In (b), for clarity only four representative CD spectra are shown to illustrate the change of the sign of the two Cotton effects associated with the maximum of UV absorption from 212 nm.

and by the decoupling of bundles of helical columns, providing a reversible "molecular rotator" motion controlled by temperature. Because this molecular rotator motion is generated by changes within the packing of bundles of helical columns,[8,30] it is most probable that these changes are concerted.

One possible mechanism that can account for the inversion of chirality at the transition from orthorhombic to hexagonal lattices is illustrated in Figure 13. The strongest possible coupling of the columns is achieved via interdigitation of the undulated periphery of helical columns with opposite handedness. In a triangular lattice, such as Φ_h^{3D}, symmetry constraints limit the column-to-column correlations in the case when all the columns have the same handedness (Figure 13). Furthermore, the symmetry of the hexagonal lattice disfavors close packing of helical columns with opposite handedness. For example, if one left and one right handed column are closely packed as shown in Figure 13, the third one, either left or right handed, cannot form a triangular close packing with the first two, because such packing will be frustrated by either the left or, respectively, the right handed column forming the initial close-packing. In the case of a lattice with "rectangular" symmetry (i.e., 2-fold, 4-fold symmetry), such packing frustrations of helical columns do not occur. Therefore, the inversion of chirality is templated by close-packing of helical columns in the low temperature $\Phi_{s\text{-}o}^{3D}$ and $\Phi_{r\text{-}c}^{io}$ phases, as suggested by the smaller lattice parameter b = 26.1 and 26.9 Å of the $\Phi_{s\text{-}o}^{3D}$ and $\Phi_{r\text{-}c}^{io}$ phases, respectively, in comparison with a = 31.2 and 29.1 Å in the Φ_h^{3D} and Φ_h^{io} phases, respectively (Figure 10).

The types of conformational changes shown in Figures 11, 12, and 13 have been shown theoretically to influence the properties of the structures, in particular of the charge transport of organic electronic materials.[31] Therefore, the proposed mechanism of self-assembly (Figure 13) has the potential, via appropriate dendritic functionalization of other aromatic groups, which exhibit increased charge transport, to reveal which combination of π-stacking distance and of φ and θ_1 angles facilitates the maximum value of the charge carrier mobility.[31]

Chiral Supramolecular Spheres. The second generation dendrimer 1,3,5-Bz-[tris(3,4,5)^{2}dm8*G2]-trisester functionalized with chiral chains self-organizes into the $Pm\bar{3}n$ cubic lattice.[21c,23,24] The relative electron density distribution (Figure 14), reconstructed using the amplitudes calculated from the powder XRD data (Figure 14a), illustrates the spherical shape of the supramolecular structures self-assembled from 1,3,5-Bz-[tris(3,4,5)^2-dm8*G2]-trisester. The CD and UV−vis spectra collected from spin-coated films exhibit the signature of a negative exciton coupling[28] (Figure 14c,d). The two Cotton effects observed, positive at 202 nm and negative at 217 nm, have roughly one-half of the intensity of the two Cotton effects observed for the first generation 1,3,5-Bz-[tris(3,4,5)dm8*G1]-trisamide dendrimer in the high temperature Φ_h^{io} phase (Figure 9). The maximum of the UV absorption, which accompanies the two Cotton effects associated with the negative exciton coupling, is observed at 212 nm in both structures (Figures 9 and 14d). These results demonstrate that the negative chirality established for the helical supramolecular columns self-assembled from the first generation 1,3,5-Bz-[tris(3,4,5)dm8*G1]-trisamide dendrimers is preserved

dx.doi.org/10.1021/ja110753s |J. Am. Chem. Soc. 2011, 133, 2311–2328

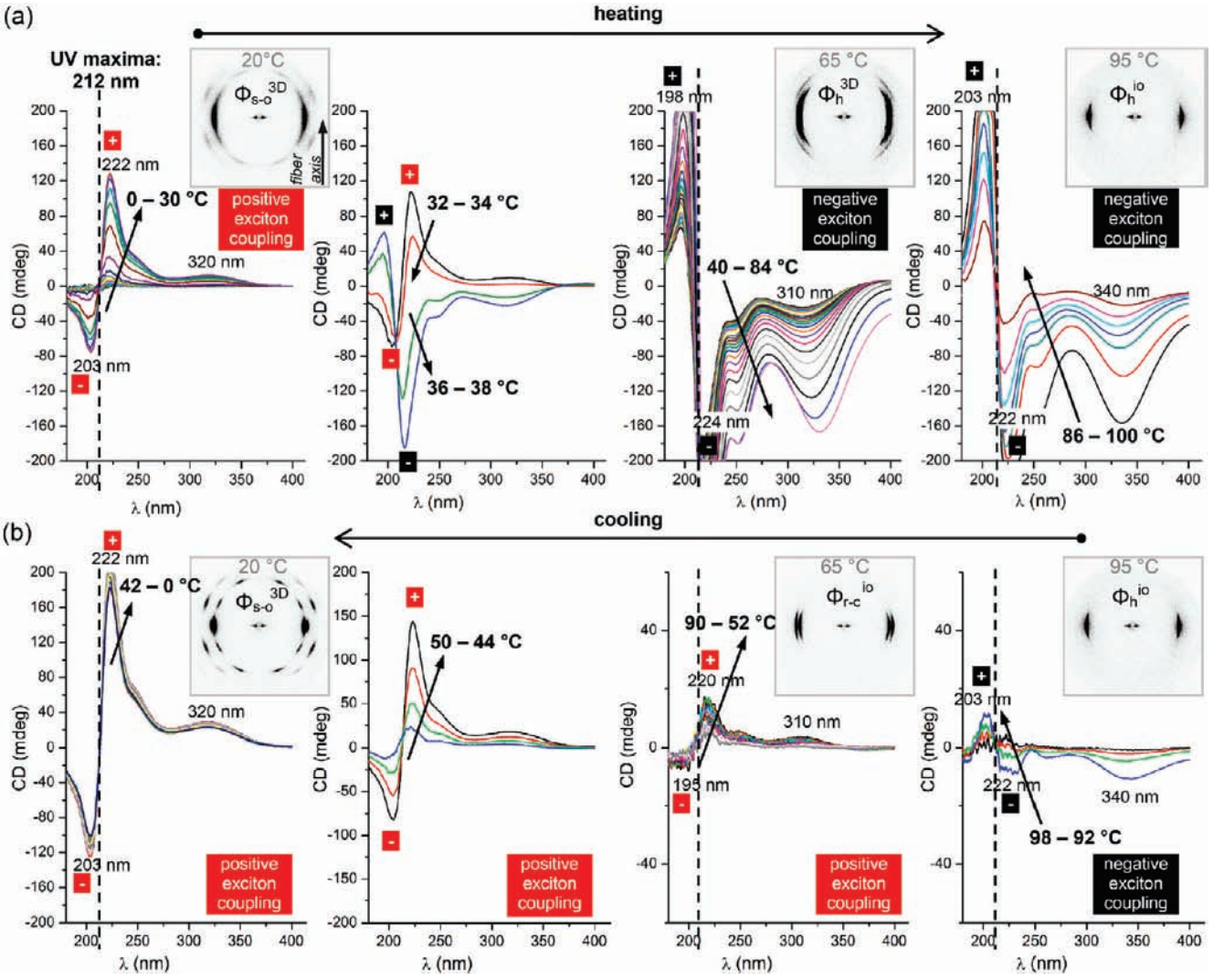

Figure 9. Temperature dependence of the CD spectra of 1,3,5-Bz-[tris(3,4,5)dm8*G1]-trisamide in spin-coated film cast from hexane (concentration = 2.0%, w/v) on heating (a) and cooling (b). Maximum of the UV absorption, representative SAXS fiber patterns, and phase assignments are indicated.

in the case of the chiral spheres self-assembled from the second generation 1,3,5-Bz-[tris(3,4,5)^{2}dm8*G2]-trisester dendrimers (Figure 14e). The relatively weak Cotton effects observed in the later structure suggest that most probably the observed CD spectrum was generated by uncorrelated chiral spheres. In other words, there is almost no chirality transfer between the supramolecular spheres. This is also supported by the observation that the maximum correlation length, ξ, of the helical packing of the 1,3,5-Bz-[tris(3,4,5)dm8*G1]-trisamide dendrimer in the high temperature Φ_h^{io} is about 8 column strata. Considering that the intensity of the Cotton effects observed for the second generation 1,3,5-Bz-[tris(3,4,5)^{2}dm8*G2]-trisester dendrimer is roughly one-half of those observed for the first generation 1,3,5-Bz-[tris-(3,4,5)dm8*G1]-trisamide dendrimer (Figures 9 and 14), then the $\xi \approx 8$ dendrimers of the later structure translate into a correlation length of the helical packing of the chiral spheres of about 4 dendrimers.

Figure 15 illustrates the direct correlation between the self-organization into columnar and cubic phases, and the primary structure of the dendrimer. Cubic phases are observed only in the second generation dendrimers with a high degree of intramolecular overcrowdedness[15c,15d] generated by their aromatic substitution pattern. These intramolecular steric constrains, indicated in Figure 15 by the color surfaces, distort the 2D close to planar conformation of the dendrimers and template a 3D propeller- (Figure 13) or crown-like[2e] (Figure 16) conformation, which in turn favor self-organization into phases with 3D periodicity (Tables 1−3).

Helical Packing of C_3-Symmetric Dendrimers. Figure 17 summarizes the packing of columnar hexagonal phases self-organized from helical supramolecular columns self-assembled from dendrimers with C_3 symmetry. In the case of columnar hexagonal phases without intercolumnar order, such as Φ_h and Φ_h^{io}, there are no limitations on the length of the helix. Furthermore, the two parameters c and φ, which uniquely define a specific type of helix,[2e] are templated only by intracolumnar interactions. The two representative examples shown in Figure 17a illustrate that in the presence of H-bonding interactions the helical parameter c increases from 3.4 to 3.8 Å and the helical parameter φ significantly increases from 12° to 60°, respectively.

In the case of columnar hexagonal phases with intercolumnar order, such as the various Φ_h^{3D} phases (Tables 1−3), the presence

dx.doi.org/10.1021/ja110753s |J. Am. Chem. Soc. 2011, 133, 2311–2328

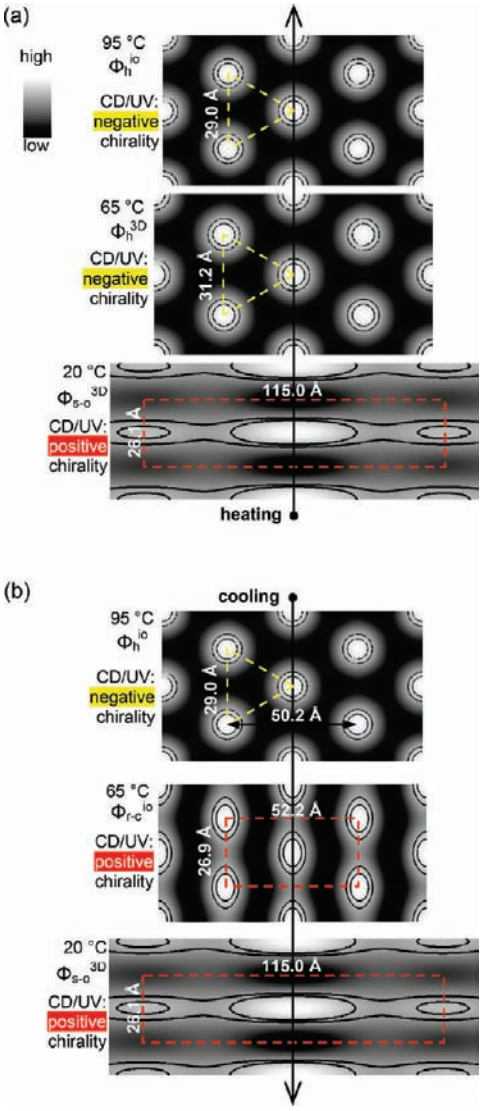

Figure 10. Relative electron density maps of 1,3,5-Bz-[tris(3,4,5)-dm8*G1]-trisamide in the columnar phases observed upon heating (a) and cooling (b). Temperature, phase, unit cell lattice dimensions (dashed lines), and correlation of the lattice symmetry with the sign of chirality established in CD/UV are indicated.

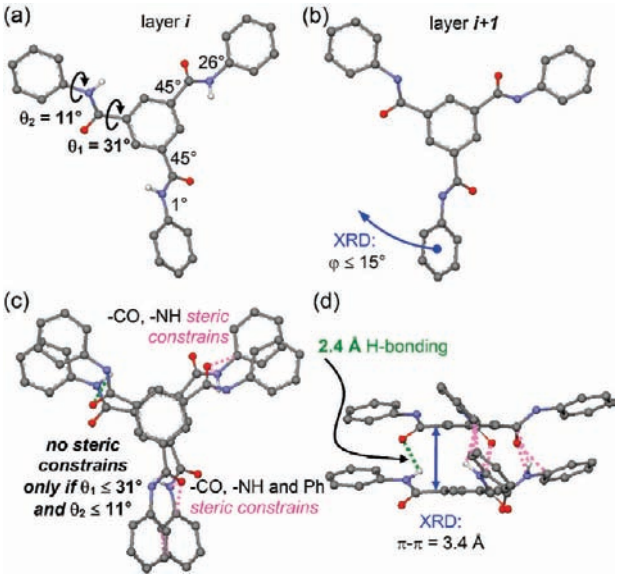

Figure 11. Molecular models of the aromatic core region in the Φ_h^{3D} phases self-assembled from 1,3,5-Bz-[tris(3,4,5)-G1]-trisamide dendrimers: three representative sets of the torsion angles θ_1 and θ_2 (a); intercolumnar correlations limit the dendrimer rotation φ from layer i to $i+1$ (b); top (c) and side (d) views of two consecutive layers. In parts c and d, the H-bonding (dotted green lines) and the steric monitoring distances are indicated.

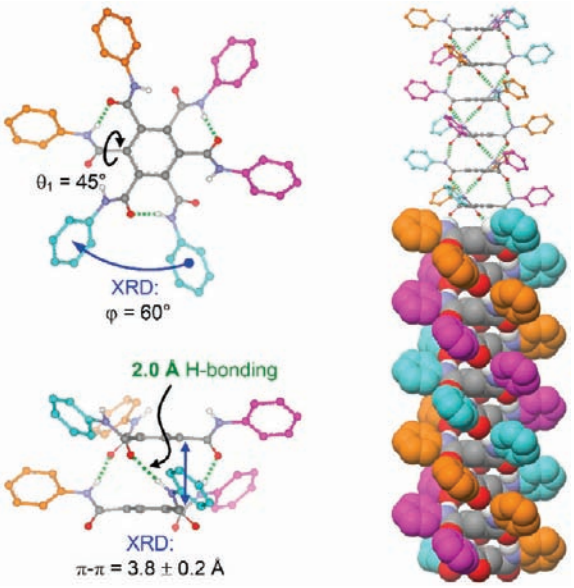

Figure 12. Molecular models illustrating the conformation of the aromatic core region of the supramolecular helical columns forming the Φ_h^{io} phase self-assembled from 1,3,5-Bz-[tris(3,4,5)12G1]-trisamide and 1,3,5-Bz-[tris(3,4,5)dm8*G1]-trisamide dendrimers.

of stronger or weaker column-to-column correlations limits the helical parameter φ. This limitation is generated by a complex mechanism that cooperatively minimizes the free energy both at the intra- and at the intercolumnar levels (Figure 17b). In Figure 17b, helical "growth" of the coupled columns, which is limited by the column-to-column steric constrains, can be followed from left to right. When this limit is achieved, the helical growth continues via two possible routes of passing this discontinuity of the helix. In the case of achiral dendrimers, the helical packing continues either by inverting the handedness or via a step-like discontinuity δ (Figure 17b, bottom). In the case of chiral dendrimers, the presence of the chiral centers typically favors one handedness. Therefore, their helical packing continues preferentially via a δ step-like discontinuity.

Interestingly, the relative electron density distributions of the Φ_h^{3D} phases observed in the chiral and achiral dendrimers, 1,3,5-Bz-[tris(3,4,5)dm8*G1]-trisamide and 1,3,5-Bz-[tris(3,4,5)12G1]-trisamide, respectively, demonstrate that there is an additional discontinuity of the helical packing at the midpoint of the helical supramolecular column along the *c*-axis (Figures 7c and SF2b). The "normal" discontinuity of the helical packing, which corresponds to the two "ends" of the column that template the *c*-axis repeat unit, can be attributed to one of the two possible mechanisms (Figure 17b). Yet this additional "mid-point" discontinuity, which exhibits a somewhat stronger modulation of the

dx.doi.org/10.1021/ja110753s |*J. Am. Chem. Soc.* 2011, 133, 2311–2328

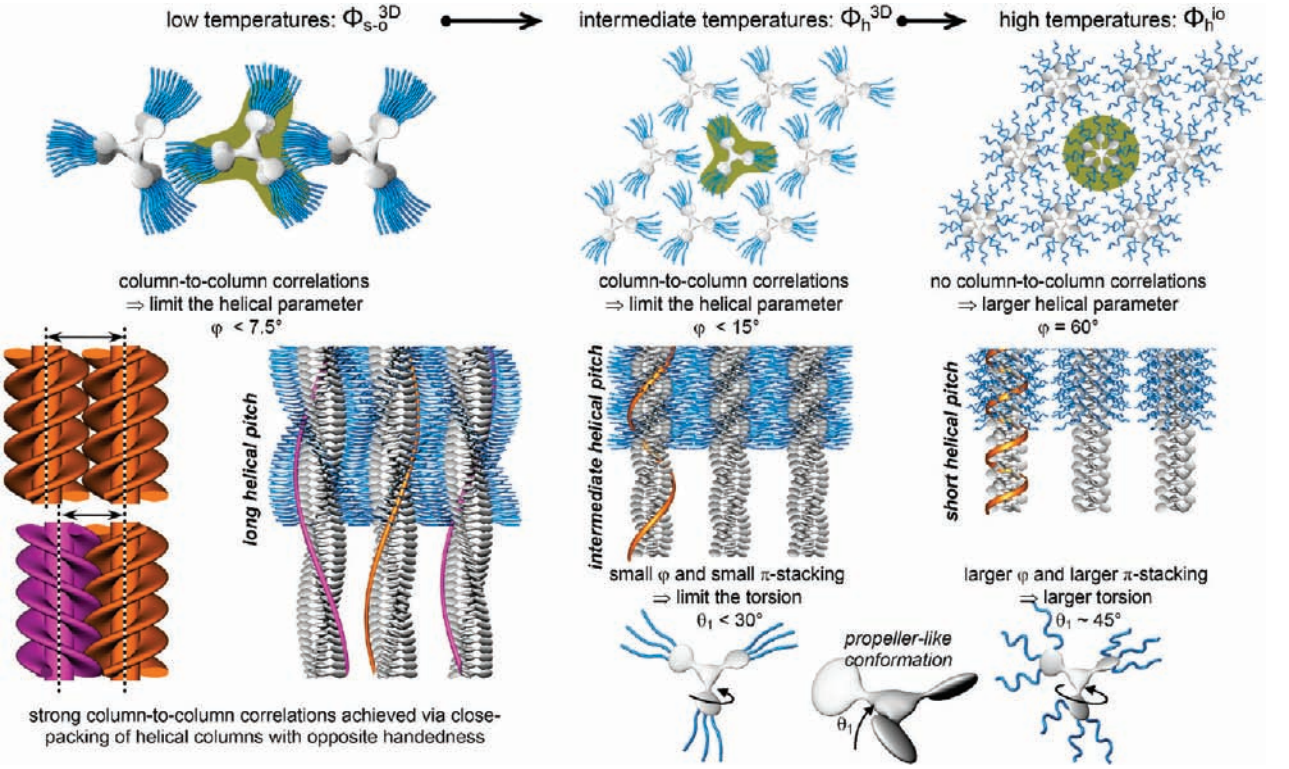

Figure 13. Changes at the molecular and supramolecular level observed upon the $\Phi_{s\text{-}o}^{3D}-\Phi_h^{3D}$ and $\Phi_h^{3D}-\Phi_h^{io}$ transitions of the supramolecular helical columns self-assembled from C_3 dendrimers.

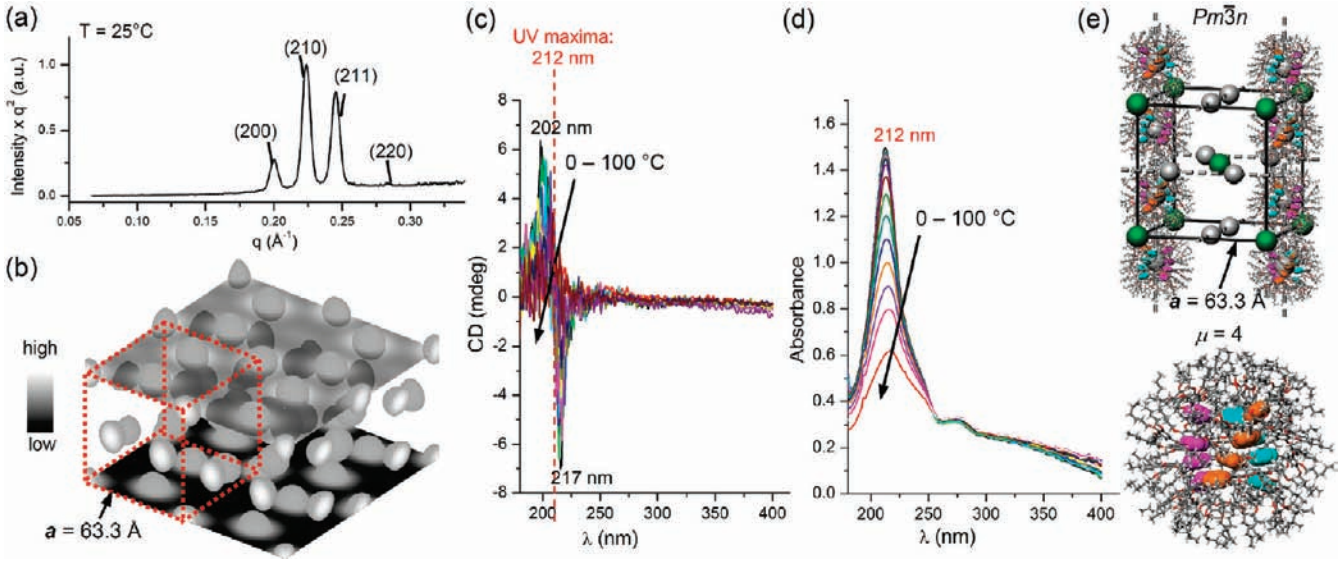

Figure 14. Powder XRD data (a), relative electron density distribution illustrating the spherical shape of the high electron density region of the supramolecular assemblies (b), CD (c), and UV−vis (d) spectra of 1,3,5-Bz-[tris(3,4,5)^{2}dm8*G2]-trisester in spin-coated film cast from hexane (concentraton = 1.2%, w/v) in the $Pm\bar{3}n$ cubic phase and molecular model of the chiral supramolecular spherical assemblies (e).

electron density in the case of the chiral dendrimer, remains unresolved. If in the case of an achiral structure the two discontinuity points of the helical packing can be attributed to helix inversion and to a helix δ step-like discontinuity, respectively, such assignment is prohibited in the case of the 1,3,5-Bz-[tris(3,4,5)dm8*G1]-trisamide dendrimer by the CD spectra (Figure 9).

In addition, the increase of the *c*-axis with more than 43%, from 54.2 Å, in the case of the 1,3,5-Bz-[tris(3,4,5)12G1]-trisamide, to 77.3 Å, in the case of 1,3,5-Bz-[tris(3,4,5)dm8*G1]-trisamide, also suggests that the two helical fragments forming the unit cell of the former structure have the same handedness. Therefore, the midpoint discontinuity is most probable a second

dx.doi.org/10.1021/ja110753s |*J. Am. Chem. Soc.* 2011, 133, 2311–2328

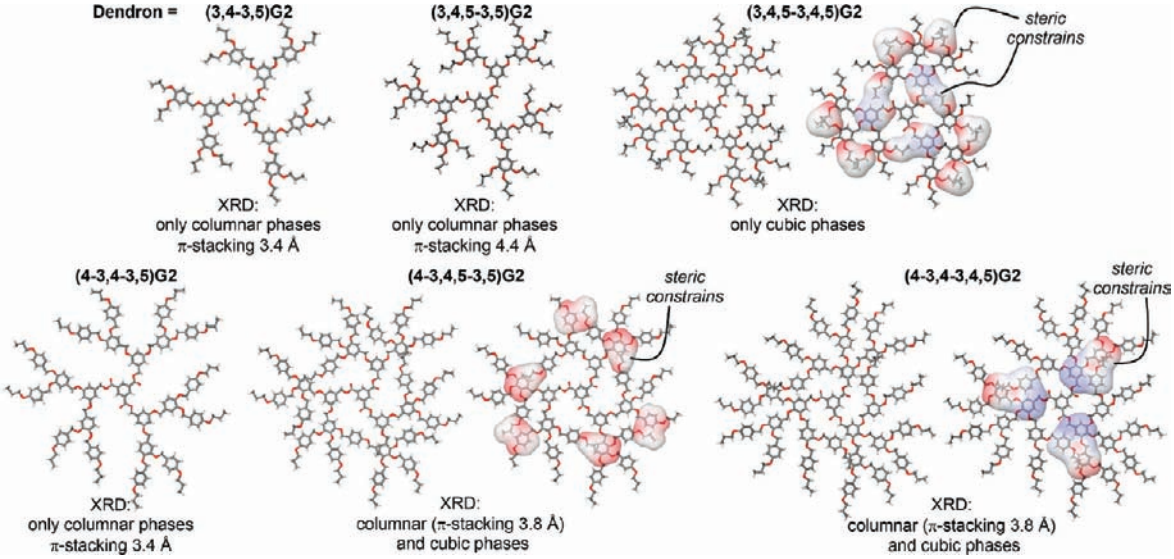

Figure 15. Correlation of the dendron substitution pattern with the self-assembly and self-organization into columnar and cubic phases for the libraries of second generation dendrimers.

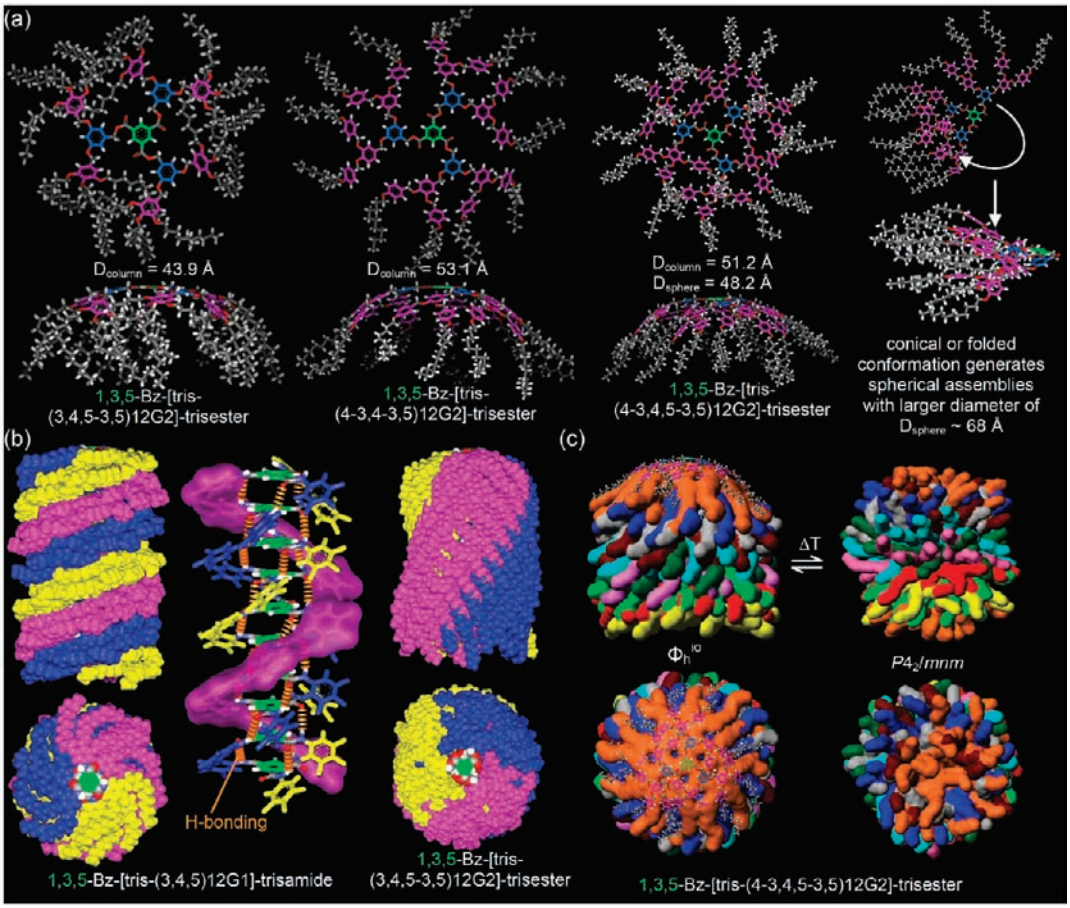

Figure 16. Molecular models of selected examples of C_3-dendrimers supporting their crown-like rather than conical conformation (a), helical supramolecular columns (b), and the column to sphere shape change at the transition from columnar hexagonal to tetragonal phase (c).

δ-step that can arise from periodic fluctuations of the helical packing generated by deviations of c, φ, and θ_1 parameters. For example, the WAXS fiber patterns collected in the Φ_h^{3D} and Φ_h^{io} phases of the 1,3,5-Bz-[tris(3,4,5)-G1]-trisamide dendrimers exhibit diffuse broad features in the region of π-stacking distance (Figures 5 and 7). This demonstrates that

dx.doi.org/10.1021/ja110753s |J. Am. Chem. Soc. 2011, 133, 2311–2328

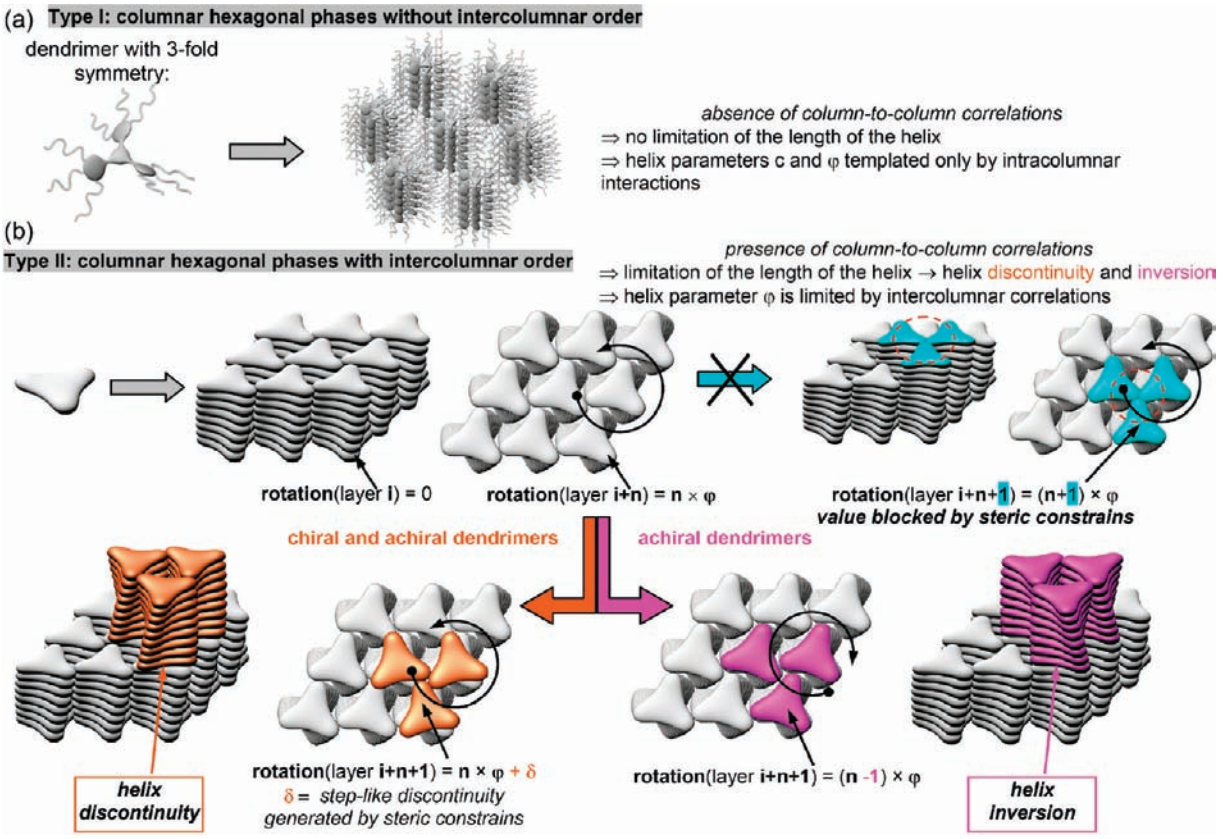

Figure 17. Helical packing of dendrimers with 3-fold symmetry self-assembled into columnar hexagonal phases without (a) and with (b) column-to-column correlations.

the stacking of the dendrimers has only short-range correlations.

CONCLUSIONS

The self-assembly of an unexpected diversity of three-dimensional columnar, cubic, and tetragonal periodic arrays from simple trisester and trisamide dendrimers with C_3-symmetry was demonstrated to be determined by different degrees of packing on the periphery of their supramolecular structures. By comparison with other classes of C_3-symmetric dendrimers,[15c,15d] the structures reported here have a significantly less-packed peripheral alkyl region and an increased conformational freedom. The combination of these two main structural characteristics was shown to generate molecular rotators, chiral spheres, helical columns with unusual long helical pitch, and facilitate the transfer, amplification, and inversion of helical chirality via transitions from strongly coupled helical columns with long helical pitch to weakly or uncoupled helical columns with short helical pitch. The mechanism of the thermal-reversible inversion of helical chirality was demonstrated to be due to the change of the lattice symmetry: negative chirality for 2D and 3D phases with triangular symmetry (columnar hexagonal) and positive chirality for 2D and 3D phases with rectangular symmetry (columnar rectangular and orthorhombic). To our knowledge, this is the first example of a reversible inversion of helical chirality in supramolecular dendrimers for which the mechanism was elucidated. The mechanism of self-assembly into the coupled or uncoupled helical columns demonstrated here provides additional pathways to tune and control the packing of helical structures via changes of the primary structure of the building block. This strategy can be used to design other molecular rotators, mechanical-like functions, and novel molecular recognition process, as well as to correlate charge transport properties[31] with changes of the molecular conformation and 3D packing. The new supramolecular structures reported here demonstrate the capability of the topology of the self-assembling dendrimer as a new and simple design strategy that is complementary to generational[7,20] and deconstruction[26] design strategies. These design strategies are required for the discovery of primary structures that provide access to new supramolecular dendrimer architectures and periodic arrays.

ASSOCIATED CONTENT

Supporting Information. Experimental procedures with complete, spectral, structural, and retrostructural analysis, and complete ref 2i. This material is available free of charge via the Internet at http://pubs.acs.org.

AUTHOR INFORMATION

Corresponding Author
percec@sas.upenn.edu

ACKNOWLEDGMENT

Financial support by the National Science Foundation (DMR-0548559 and DMR-0520020) and the P. Roy Vagelos Chair at Penn is gratefully acknowledged. B.M.R. gratefully

acknowledges funding from an NSF Graduate Research Fellowship and ACS Division of Organic Chemistry Graduate Fellowship (Roche).

REFERENCES

(1) Percec, V.; Dulcey, A. E.; Balagurusamy, V. S. K.; Miura, Y.; Smidrkal, J.; Peterca, M.; Nummelin, S.; Edlund, U.; Hudson, S. D.; Heiney, P. A.; Hu, D. A.; Magonov, S. N.; Vinogradov, S. A. *Nature* **2004**, *430*, 764–768.

(2) (a) Soininen, A. J.; Kasemi, E.; Schlüter, A. D.; Ikkala, O.; Ruokolainen, J.; Mezzenga, R. *J. Am. Chem. Soc.* **2010**, *132*, 10882–10890. (b) Astruc, D.; Boisselier, E.; Ornelas, C. *Chem. Rev.* **2010**, *110*, 1857–1959. (c) Rosen, B. M.; Wilson, C. J.; Wilson, D. A.; Peterca, M.; Imam, M. R.; Percec, V. *Chem. Rev.* **2009**, *109*, 6275–6540. (d) Lehmann, M.; Jahr, M.; Donnio, B.; Graf, R.; Gemming, S.; Popov, I. *Chem.-Eur. J.* **2008**, *14*, 3562–3576. (e) Peterca, M.; Percec, V.; Imam, M. R.; Leowanawat, P.; Morimitsu, K.; Heiney, P. A. *J. Am. Chem. Soc.* **2008**, *130*, 14840–14852. (f) Grayson, S. M.; Frechet, J. M. J. *Chem. Rev.* **2001**, *101*, 3819–3867. (g) Donnio, B.; Buathong, S.; Bury, I.; Guillon, D. *Chem. Soc. Rev.* **2007**, *36*, 1495–1513. (h) Marcos, M.; Martin-Rapun, R.; Omenat, A.; Serrano, J. L. *Chem. Soc. Rev.* **2007**, *36*, 1889–1901. (i) Percec, V.; et al. *Science* **2010**, *328*, 1009–1014.

(3) (a) Hill, D. J.; Mio, M. J.; Prince, R. B.; Hughes, T. S.; Moore, J. S. *Chem. Rev.* **2001**, *101*, 3893–4011. (b) Vera, F.; Tejedor, R. M.; Romero, P.; Barbera, J.; Ros, M. B.; Serrano, J. L.; Sierra, T. *Angew. Chem., Int. Ed.* **2007**, *46*, 1873–1877. (c) Hill, J. P.; Jin, W. S.; Kosaka, A.; Fukushima, T.; Ichihara, H.; Shimomura, T.; Ito, K.; Hashizume, T.; Ishii, N.; Aida, T. *Science* **2004**, *304*, 1481–1483. (d) Kato, T.; Mizoshita, N.; Kishimoto, K. *Angew. Chem., Int. Ed.* **2006**, *45*, 38–68. (e) De Greef, T. F. A.; Smulders, M. M. J.; Wolffs, M.; Schenning, A.; Sijbesma, R. P.; Meijer, E. W. *Chem. Rev.* **2009**, *109*, 5687–5754. (f) Cho, B. K.; Jain, A.; Gruner, S. M.; Wiesner, U. *Science* **2004**, *305*, 1598–1601. (g) Don, X.; Pisula, W.; Wu, J.; Bodwell, G. J.; Müllen, K. *Chem.-Eur. J.* **2008**, *14*, 240–249. (h) Smulders, M. M. J.; Schenning, A.; Meijer, E. W. *J. Am. Chem. Soc.* **2008**, *130*, 606–611.

(4) (a) Shibaev, V.; Bobrovsky, A.; Boiko, N. *Prog. Polym. Sci.* **2003**, *28*, 729–836. (b) Brettar, J.; Burgi, T.; Donnio, B.; Guillon, D.; Klappert, R.; Scharf, T.; Deschenaux, R. *Adv. Funct. Mater.* **2006**, *16*, 260–267. (c) Campidelli, S.; Brandmuller, T.; Hirsch, A.; Saez, I. M.; Goodby, J. W.; Deschenaux, R. *Chem. Commun.* **2006**, 4282–4284.

(5) Lehn, J. M. *Angew. Chem., Int. Ed. Engl.* **1990**, *29*, 1304–1319.

(6) (a) Fenniri, H.; Deng, B. L.; Ribbe, A. E. *J. Am. Chem. Soc.* **2002**, *124*, 11064–11072. (b) Jin, W.; Fukushima, T.; Niki, M.; Kosaka, A.; Ishii, N.; Aida, T. *Proc. Natl. Acad. Sci. U.S.A.* **2005**, *102*, 10801–10806. (c) Yang, W. Y.; Lee, E.; Lee, M. *J. Am. Chem. Soc.* **2006**, *128*, 3484–3485.

(7) Percec, V.; Won, B. C.; Peterca, M.; Heiney, P. A. *J. Am. Chem. Soc.* **2007**, *129*, 11265–11278.

(8) Percec, V.; Rudick, J. G.; Peterca, M.; Heiney, P. A. *J. Am. Chem. Soc.* **2008**, *130*, 7503–7508.

(9) (a) Percec, V.; Glodde, M.; Bera, T. K.; Miura, Y.; Shiyanovskaya, I.; Singer, K. D.; Balagurusamy, V. S. K.; Heiney, P. A.; Schnell, I.; Rapp, A.; Spiess, H. W.; Hudson, S. D.; Duan, H. *Nature* **2002**, *419*, 384–387. (b) Nguyen, T. Q.; Martel, R.; Bushey, M.; Avouris, P.; Carlsen, A.; Nuckolls, C.; Brus, L. *Phys. Chem. Chem. Phys.* **2007**, *9*, 1515–1532. (c) Murphy, A. R.; Fréchet, J. M. J. *Chem. Rev.* **2007**, *107*, 1066–1096.

(10) (a) Elemans, J.; Rowan, A. E.; Nolte, R. J. M. *J. Mater. Chem.* **2003**, *13*, 2661–2670. (b) Rapp, A.; Schnell, I.; Sebastiani, D.; Brown, S. P.; Percec, V.; Spiess, H. W. *J. Am. Chem. Soc.* **2003**, *125*, 13284–13297.

(11) (a) Li, L. S.; Jiang, H. Z.; Messmore, B. W.; Bull, S. R.; Stupp, S. I. *Angew. Chem., Int. Ed.* **2007**, *46*, 5873–5876. (b) Ernst, J. T.; Becerril, J.; Park, H. S.; Yin, H.; Hamilton, A. D. *Angew. Chem., Int. Ed.* **2003**, *42*, 535–539.

(12) Würthner, F.; Chen, Z. J.; Hoeben, F. J. M.; Osswald, P.; You, C. C.; Jonkheijm, P.; von Herrikhuyzen, J.; Schenning, A.; van der Schoot, P.; Meijer, E. W.; Beckers, E. H. A.; Meskers, S. C. J.; Janssen, R. A. J. *J. Am. Chem. Soc.* **2004**, *126*, 10611–10618.

(13) Yashima, E.; Maeda, K.; Nishimura, T. *Chem.-Eur. J.* **2004**, *10*, 42–51.

(14) Rowan, A. E.; Nolte, R. J. M. *Angew. Chem., Int. Ed.* **1998**, *37*, 63–68.

(15) (a) van Gorp, J. J.; Vekemans, J.; Meijer, E. W. *J. Am. Chem. Soc.* **2002**, *124*, 14759–14769. (b) Alam, M. A.; Motoyanagi, J.; Yamamoto, Y.; Fukushima, T.; Kim, J.; Kato, K.; Takata, M.; Saeki, A.; Seki, S.; Tagawa, S.; Aida, T. *J. Am. Chem. Soc.* **2009**, *131*, 17722–17723. (c) Percec, V.; Imam, M. R.; Peterca, M.; Wilson, D. A.; Heiney, P. A. *J. Am. Chem. Soc.* **2009**, *131*, 1294–1304. (d) Percec, V.; Imam, M. R.; Peterca, M.; Wilson, D. A.; Graf, R.; Spiess, H. W.; Balagurusamy, V. S. K.; Heiney, P. A. *J. Am. Chem. Soc.* **2009**, *131*, 7662–7677. (e) Cordovilla, C.; Coco, S.; Espinet, P.; Donnio, B. *J. Am. Chem. Soc.* **2010**, *132*, 1424–1431.

(16) (a) Peterca, M.; Imam, M. R.; Leowanawat, P.; Rosen, B. M.; Wilson, D. A.; Wilson, C. J.; Zeng, X. B.; Ungar, G.; Heiney, P. A.; Percec, V. *J. Am. Chem. Soc.* **2010**, *132*, 11288–11305. (b) Peterca, M.; Percec, V.; Dulcey, A. E.; Nummelin, S.; Korey, S.; Ilies, M.; Heiney, P. A. *J. Am. Chem. Soc.* **2006**, *128*, 6713–6720.

(17) (a) Fujiki, M. *J. Am. Chem. Soc.* **2000**, *122*, 3336–3343. (b) Johnson, R. S.; Yamazaki, T.; Kovalenko, A.; Fenniri, H. *J. Am. Chem. Soc.* **2007**, *129*, 5735–5743.

(18) (a) Koumura, N.; Zijlstra, R. W. J.; van Delden, R. A.; Harada, N.; Feringa, B. L. *Nature* **1999**, *401*, 152–155. (b) van Delden, R. A.; ter Wiel, M. K. J.; Pollard, M. M.; Vicario, J.; Koumura, N.; Feringa, B. L. *Nature* **2005**, *437*, 1337–1340.

(19) (a) Aparicio, F.; Vicente, F.; Sanchez, L. *Chem. Commun.* **2010**, *46*, 8356–8358. (b) Yamamoto, T.; Fukushima, T.; Kosaka, A.; Jin, W.; Yamamoto, Y.; Ishii, N.; Aida, T. *Angew. Chem., Int. Ed.* **2008**, *47*, 1672–1675. (c) Nam, S. R.; Lee, H. Y.; Hong, J. I. *Chem.-Eur. J.* **2008**, *14*, 6040–6043. (d) Ajayaghosh, A.; Varghese, R.; Mahesh, S.; Praveen, V. K. *Angew. Chem., Int. Ed.* **2006**, *45*, 7729–7732. (e) Ajayaghosh, A.; Varghese, R.; George, S. J.; Vijayakumar, C. *Angew. Chem., Int. Ed.* **2006**, *45*, 1141–1144.

(20) (a) Percec, V.; Cho, W. D.; Ungar, G.; Yeardley, D. J. P. *J. Am. Chem. Soc.* **2001**, *123*, 1302–1315. (b) Percec, V.; Mitchell, C. M.; Cho, W. D.; Uchida, S.; Glodde, M.; Ungar, G.; Zeng, X. B.; Liu, Y. S.; Balagurusamy, V. S. K.; Heiney, P. A. *J. Am. Chem. Soc.* **2004**, *126*, 6078–6094. (c) Percec, V.; Peterca, M.; Sienkowska, M. J.; Ilies, M. A.; Aqad, E.; Smidrkal, J.; Heiney, P. A. *J. Am. Chem. Soc.* **2006**, *128*, 3324–3334. (d) Rosen, B. M.; Wilson, D. A.; Wilson, C. J.; Peterca, M.; Won, B. C.; Huang, C. H.; Lipski, L. R.; Zeng, X. B.; Ungar, G.; Heiney, P. A.; Percec, V. *J. Am. Chem. Soc.* **2009**, *131*, 17500–17521.

(21) (a) Percec, V.; Cho, W. D.; Ungar, G. *J. Am. Chem. Soc.* **2000**, *122*, 10273–10281. (b) Percec, V.; Cho, W. D.; Mosier, P. E.; Ungar, G.; Yeardley, D. J. P. *J. Am. Chem. Soc.* **1998**, *120*, 11061–11070. (c) Balagurusamy, V. S. K.; Ungar, G.; Percec, V.; Johansson, G. *J. Am. Chem. Soc.* **1997**, *119*, 1539–1555. (d) Johansson, G.; Percec, V.; Ungar, G.; Abramic, D. *J. Chem. Soc., Perkin Trans. 1* **1994**, 447–459. (e) Tapia, R.; Torres, G.; Valderrama, J. A. *Synth. Commun.* **1986**, *16*, 681–687.

(22) (a) Percec, V.; Imam, M. R.; Bera, T. K.; Balagurusamy, V. S. K.; Peterca, M.; Heiney, P. A. *Angew. Chem., Int. Ed.* **2005**, *44*, 4739–4745. (b) Percec, V.; Ahn, C. H.; Bera, T. K.; Ungar, G.; Yeardley, D. J. P. *Chem.-Eur. J.* **1999**, *5*, 1070–1083. (c) Percec, V.; Bera, T. K.; Glodde, M.; Fu, Q. Y.; Balagurusamy, V. S. K.; Heiney, P. A. *Chem.-Eur. J.* **2003**, *9*, 921–935.

(23) Cho, B. K.; Jain, A.; Gruner, S. M.; Wiesner, U. *Science* **2004**, *305*, 1598–1601.

(24) (a) Hudson, S. D.; Jung, H. T.; Percec, V.; Cho, W. D.; Johansson, G.; Ungar, G.; Balagurusamy, V. S. K. *Science* **1997**, *278*, 449–452. (b) Percec, V.; Ahn, C. H.; Ungar, G.; Yeardley, D. J. P.; Möller, M.; Sheiko, S. S. *Nature* **1998**, *391*, 161–164. (c) Dukeson, D. R.; Ungar, G.; Balagurusamy, V. S. K.; Percec, V.; Johansson, G. A.; Glodde, M. *J. Am. Chem. Soc.* **2003**, *125*, 15974–15980. (d) Percec, V.; Peterca, M.; Dulcey, A. E.; Imam, M. R.; Hudson, S. D.; Nummelin S.; Adelman, P.; Heiney, P. A. *J. Am. Chem. Soc.* **2008**, *130*, 13079–13094.

(25) (a) Ungar, G.; Liu, Y. S.; Zeng, X. B.; Percec, V.; Cho, W. D. *Science* **2003**, *299*, 1208–1211. (b) Lee, S.; Bluemle, M. J.; Bates, F. S.

Science **2010**, *330*, 349–353. (c) Peterca, M.; Percec, V. *Science* **2010**, *330*, 333–334.

(26) Rosen, B. M.; Peterca, M.; Huang, C.; Zeng, X.; Ungar, G.; Percec, V. *Angew. Chem., Int. Ed.* **2010**, *49*, 7002–7005.

(27) Ungar, G.; Percec, V.; Holerca, M. N.; Johansson, G.; Heck, J. A. *Chem.-Eur. J.* **2000**, *6*, 1258–1266.

(28) Berova, N.; Di Bari, L.; Pescitelli, G. *Chem. Soc. Rev.* **2007**, *36*, 914–931.

(29) Levelut, A. M.; Malthête, J.; Collet, A. *J. Phys. (Paris)* **1986**, *47*, 351–357.

(30) Feringa, B. L.; Browne, W. R. *Nat. Nanotechnol.* **2008**, *3*, 383–384.

(31) (a) Lemaur, V.; Da Silva Filho, D. A.; Coropceanu, V.; Lehmann, M.; Geerts, Y.; Piris, J.; Debije, M. G.; Van de Craats, A. M.; Senthilkumar, K.; Siebbeles, L. D. A.; Warman, J. M.; Bredas, J. L.; Cornil, J. *J. Am. Chem. Soc.* **2004**, *126*, 3271–3279. (b) Stals, P. J. M.; Everts, J. C.; de Bruijn, R.; Filot, I. A. W.; Smulders, M. M. J.; Martin-Rapun, R.; Pidko, E. A.; de Greef, T. F. A.; Palmans, A. R. A.; Meijer, E. W. *Chem.-Eur. J.* **2010**, *16*, 810–821. (c) Demenev, A.; Eichhorn, S. H.; Taerum, T.; Perepichka, D. F.; Patwardhan, S.; Grozema, F. C.; Siebbeles, L. D. A.; Klenkler, R. *Chem. Mater.* **2010**, *22*, 1420–1428.